Open Access Articles

# *Influence of total organic carbon deposition on the inventory of gas hydrate in the Indian continental margins*

The Faculty of Oregon State University has made this article openly available.
Please share how this access benefits you. Your story matters.



| | |
|---|---|
| **Citation** | Johnson, J. E., Phillips, S. C., Torres, M. E., Piñero, E., Rose, K. K., & Giosan, L. (2014). Influence of total organic carbon deposition on the inventory of gas hydrate in the Indian continental margins. Marine and Petroleum Geology, 58, 406-424. doi:10.1016/j.marpetgeo.2014.08.021 |
| **DOI** | 10.1016/j.marpetgeo.2014.08.021 |
| **Publisher** | Elsevier |
| **Version** | Version of Record |
| **Terms of Use** | http://cdss.library.oregonstate.edu/sa-termsofuse |

Marine and Petroleum Geology 58 (2014) 406–424

Contents lists available at ScienceDirect

Marine and Petroleum Geology

journal homepage: www.elsevier.com/locate/marpetgeo

Research paper

# Influence of total organic carbon deposition on the inventory of gas hydrate in the Indian continental margins

Joel E. Johnson [a, *], Stephen C. Phillips [a], Marta E. Torres [b], Elena Piñero [c], Kelly K. Rose [d], Liviu Giosan [e]

[a] Department of Earth Sciences, University of New Hampshire, Durham, NH, USA
[b] College of Earth, Oceanic and Atmospheric Sciences, Oregon State University, Corvallis, OR, USA
[c] GEOMAR, Helmholtz Centre for Ocean Research Kiel, Wischhofstrasse 1-3, Kiel D-24148, Germany
[d] Office of Research and Development, National Energy Technology Laboratory, Albany, OR, USA
[e] Department of Geology and Geophysics, Woods Hole Oceanographic Institution, Woods Hole, MA, USA

ARTICLE INFO

*Article history:*
Received 11 July 2014
Received in revised form
27 August 2014
Accepted 28 August 2014
Available online 6 September 2014

*Keywords:*
TOC
C/N
Organic carbon isotopes
Bay of Bengal
Krishna–Godavari
Mahanadi
Andaman accretionary wedge
Kerala–Konkan

ABSTRACT

Total organic carbon (TOC) content of marine sediments represents residual carbon, originally derived from terrestrial and marine sources, which has survived seafloor and shallow subseafloor diagenesis. Ultimately, its preservation below the sulfate reduction zone in marine sediments drives methanogenesis. Within the gas hydrate stability zone (GHSZ), methane production along continental margins can supersaturate pore fluids and lead to the formation of gas hydrate. In this paper we examine the inventory and sources of TOC in sediments collected from four regions within the GHSZ along the Indian continental margins. The recovered sediments vary in age from Oligocene to recent. Mean TOC abundance is greatest in the Krishna–Godavari (K–G) Basin and decreases progressively to the Mahanadi basin, Andaman wedge, and Kerala–Konkan (K–K) Basin. This decrease in TOC is matched by a progressive increase in biogenic $CaCO_3$ and increasing distance from terrestrial sources of organic matter and lithogenic materials. Organic carbon sources inferred from C/N and $\delta^{13}C_{TOC}$ range from terrestrial (K–G Basin) to mixed marine and terrestrial (Mahanadi Basin), to marine dominant (Andaman wedge and K–K Basin). In the K–G Basin, variation in the bulk $\delta^{13}C_{TOC}$ is consistent with changes in $C_3$ and $C_4$ vegetation driven by monsoon variability on glacial-interglacial timescales, whereas in the Mahanadi Basin a shift in the $\delta^{13}C_{TOC}$ likely reflects the onset of $C_4$ plant deposition in the Late Miocene. A large shift the $\delta^{13}C_{TOC}$ in the K–K basin is consistent with a change from $C_3$ to $C_4$ dominated plants during the middle Miocene. We observe a close relationship between TOC content and gas hydrate saturation, but consider the role of sedimentation rates on the preservation of TOC in the zone of methanogenesis and advective flow of methane from depth. Although TOC contents are sufficient for *in situ* methanogenesis at all the sites where gas hydrates were observed or inferred from proxy data, seismic, borehole log, pressure core, and gas composition data coupled with relatively high observed gas hydrate saturations suggest that advective gas transport may also play a role in the saturation of methane and the formation of gas hydrates in these regions. Although TOC content may be a first order indicator for gas hydrate potential, the structural and stratigraphic geologic environment along a margin will most likely dictate where the greatest gas hydrate saturations will occur.

© 2014 Elsevier Ltd. All rights reserved.

## 1. Introduction

Marine gas hydrates form and accumulate within the gas hydrate stability zone (GHSZ) in continental margin sediments with sufficient methane concentrations. Methane is generated from microbial degradation of organic carbon (<50 °C), from thermogenic decomposition of organic carbon at depth (80–150 °C) or from the conversion of heavier hydrocarbons to methane at temperatures >150 °C (Claypool and Kvenvolden, 1983). Gas hydrates, or methane hydrates, are most commonly formed from microbial methane, which is generated by methanogenesis from sedimentary organic carbon (Kvenvolden, 1993), and have been sampled and/or inferred in all of the global oceans (Collett et al., 2009). Thermogenic gas hydrates are less common, but have been observed for

* Corresponding author. Department of Earth Sciences, University of New Hampshire, 56 College Rd., Durham, NH 03824, USA. Tel.: +1 603 862 4080; fax: +1 603 862 2649.
*E-mail address:* joel.johnson@unh.edu (J.E. Johnson).

http://dx.doi.org/10.1016/j.marpetgeo.2014.08.021
0264-8172/© 2014 Elsevier Ltd. All rights reserved.

example in the Gulf of Mexico (Brooks et al., 1984), Caspian Sea (Ginsburg and Soloviev, 1998), on the Northern Cascadia margin (Pohlman et al., 2005), and in the Arctic Fram Strait (Smith et al., 2014). In addition, abiotic marine gas hydrates derived from the serpentinization of ultramafic rocks in oceanic crust may also exist in the Arctic Ocean (Rajan et al., 2012).

Methane migration into and within the GHSZ occurs through diffuse intragranular flow and/or advective flow through fractures, faults, or stratigraphic conduits (e.g. Carson and Screaton, 1998; Tréhu et al., 2004). Gas hydrates may persist through time along continental margins as long as (1) there is a source of methane, (2) short term pertubations (e.g. T, P, or salinity changes; Sloan and Koh, 2008) are recoverable (methane losses are balanced by inputs from depth), and (3) there is some holding capacity for methane to accumulate as gas hydrate in the GHSZ (e.g. significant host porosity and permeability; Lorenson, 2000; Xu and Ruppel, 1999). Gas hydrates can form and accumulate in unconsolidated to semi-lithified marine sediments of various stratigraphic ages, but are restricted to and maintained in the uppermost few hundred meters of sediment within the GHSZ along continental margins. In this environment high sedimentation and subsidence rates can result in the efficient burial and conversion of organic carbon to hydrocarbons and the continued upward migration of the GHSZ with time.

The global predominance of microbial methane in marine gas hydrate systems suggests that low temperature diagenetic alterations of organic matter in continental margin sediments plays a critical role in methanogenesis and the accumulation of gas hydrate within the gas hydrate stability zone (Kvenvolden, 1995). Methane in gas hydrates can be formed *in situ* from methanogenesis of the local organic carbon and/or be formed *ex situ* by either microbial or thermogenic gas generated at depth and advected upward toward or within the GHSZ. In a comparison study of TOC content and observed gas hydrate from several Pacific and Atlantic Ocean continental margins, Waseda (1998) suggests a minimum of 0.5 wt. % TOC is needed to fuel methanogenesis sufficiently to produce methane in excess of saturation and precipitate *in situ* gas hydrate. Using the modeling approach of Davie and Buffett (2001), Klauda and Sandler (2005) suggest a similar minimum TOC (>0.4 wt. %) to form *in situ* gas hydrates. Although Clayton (1992) also suggests significant microbial gas generation occurs at TOC contents >0.5 wt. %, he notes that only 0.2 wt. % is required to result in a free gas phase in sediments with 30% porosity at a 1 km burial depth. Kastner (2001) also suggests marine organic matter dominated settings with only 0.1 wt. % TOC could generate significant (~200 mM) methane concentrations in pore waters. Using data and observations from the northern Cascadia margin, Pohlman et al. (2009) suggests rather than the amount of TOC, it is the bioavailability of that TOC that may be important for *in situ* methanogenesis and gas hydrate formation. The bioavailability of organic carbon for methanogenesis in marine sediments is a function of the sedimentation (burial) rate (Stein, 1990), which affects the exposure time of the organic carbon to aerobic oxidation and sulfate reduction, and the type of organic carbon, with marine organic matter more labile than terrestrial (Burdige, 2005). Consistent with these observations, pore water data and numerical modeling show that elevated saturations of >1% observed in the Krishna–Godavari Basin offshore India, at sites with no evidence for fluid advection, may be the result of higher rates of *in situ* organic matter degradation and methanogenesis related to the high, non-steady state sedimentation rates across the basin (Solomon et al., 2014). In addition, sediments with low TOC content could host gas hydrates if the source of the gas is *ex situ* and delivered to the host via advective flow. Waseda and Uchida (2004) argue that passive margin environments like the Blake Ridge on the U.S. margin, may be dominated by *in situ* formed gas hydrate, due to the fine grained nature of the sediments and pervasive, diffuse fluid flow, resulting from the lack of significant deformation to focus gas migration upward and into the GHSZ. Paull et al. (1994), however, suggested some migration of gas from depth could occur at Blake Ridge and along other margins via gas hydrate recycling through time, which could resupply the GHSZ with *ex situ* microbial methane and precipitate gas hydrate. In active margin accretionary wedge environments (e.g. Cascadia, Nankai Trough, Chile) and on deformed passive margins, such as those influenced by salt or shale tectonics (e.g. Gulf of Mexico, Krishna–Godavari Basin), deformation and abundant stratigraphic and structural conduits for fluid flow help supply the GHSZ with deeper sources of methane, both of biogenic and thermogenic origins (e.g. Liu and Flemings, 2006; Tréhu et al., 2004). In these active margin/deformed margin settings, gas hydrate saturations locally can be very high, due to the concentrating effect of supplying the GHSZ with methane beyond that produced by *in situ* methanogenesis. For this reason, the highest gas hydrate saturation identified to date (near 100% for seafloor gas hydrate mounds), typically involve advection of methane in the gas phase along faults, fractures, or high porosity and permeability lithologic facies (Torres et al., 2008, 2011). In many of these advection-dominated environments, some of the excess advective methane can also bypass the GHSZ (Liu and Flemings, 2006; Smith et al., 2014), and be vented into the ocean, producing bubble plumes commonly imaged acoustically in the water column along many continental margins (e.g. Heeshen et al., 2003; Gardner et al., 2009; Weber et al., 2014).

If TOC preservation within the seafloor has been relatively constant over geologic timescales (i.e. the depositional environment has not changed significantly) the TOC content of shallow sediments within the GHSZ could be representative of deeper source TOC for *ex situ* produced gas and thus be a good first order indicator for overall (microbial or thermogenic) gas hydrate potential. On continental margins with consistent and high wt % TOC preserved in the sediments over geologic timescales, hydrocarbon (petroleum and gas) systems develop from this TOC (e.g. Gulf of Mexico, USA, Krishna–Godavari Basin, India). Advection of microbial and/or thermogenic gas along faults or stratigraphic conduits sourced in deeper reservoirs is often responsible for significant accumulations of gas hydrate in the subsurface (e.g. Tréhu et al., 2004; Riedel et al., 2010) and escape of gases through the GHSZ (Liu and Flemings, 2006, 2007; Torres et al., 2004, 2011). Integration of several variables, including TOC content (0.2–5 wt %), rates of sedimentation and methanogenesis, and host porosity and permeability, into the geochemical reaction transport model of Wallmann et al. (2012) suggest that gas hydrate saturations greater than 3% pore volume must be generated by advective delivery of dissolved or gaseous methane from depth.

In this paper we document the spatial and temporal variability of bulk TOC and organic carbon sources from C/N ratios and $\delta^{13}C_{TOC}$ from long sediment cores collected within the GHSZ along the continental margins of peninsular India and in the Andaman Sea during the 2006 National Gas Hydrate Program of India (NGHP) Expedition 01. We integrate these data with core lithology and sedimentation rates in order to assess the role of TOC in the documented gas hydrate occurrence at these sites. Our results show the general trend that higher TOC contents track with greater gas hydrate saturations. However, the sedimentation patterns, specifically rapid deposition of mass transport deposits (MTDs), regulates the amount of time TOC spends in the sulfate

reduction zone and consequently the delivery of labile TOC to the methanogenic zone (Solomon et al., 2014). Furthermore, the geologic setting in each region dictates the relative role of advective, *ex situ*, methane sources to the GHSZ.

## 2. Geologic setting and NGHP-01 core stratigraphy

During the NGHP-01 Expedition four regions were drilled and cored within Indian territorial waters. Three of these regions are located along peninsular India's passive continental margins within the Krishna–Godavari (K–G) and Mahanadi sedimentary basins and within the distal K–K basin, and the fourth is located on the active Sunda subduction zone margin in the Andaman accretionary wedge (Fig. 1). Below we describe the geologic setting and stratigraphy in each of these regions.

### 2.1. Krishna–Godavari and Mahanadi Basins

The Krishna–Godavari (K–G) and Mahanadi Basins are two of five pericratonic basins along the eastern Indian margin that formed during the Late Jurassic rifting of the Indian and Australia–Antarctic plates (Powell et al., 1988; Ramana et al., 2001; Subrahmanyam and Chand, 2001; Radhakrishna et al., 2012). The fault structure in these basins is characterized by horsts and

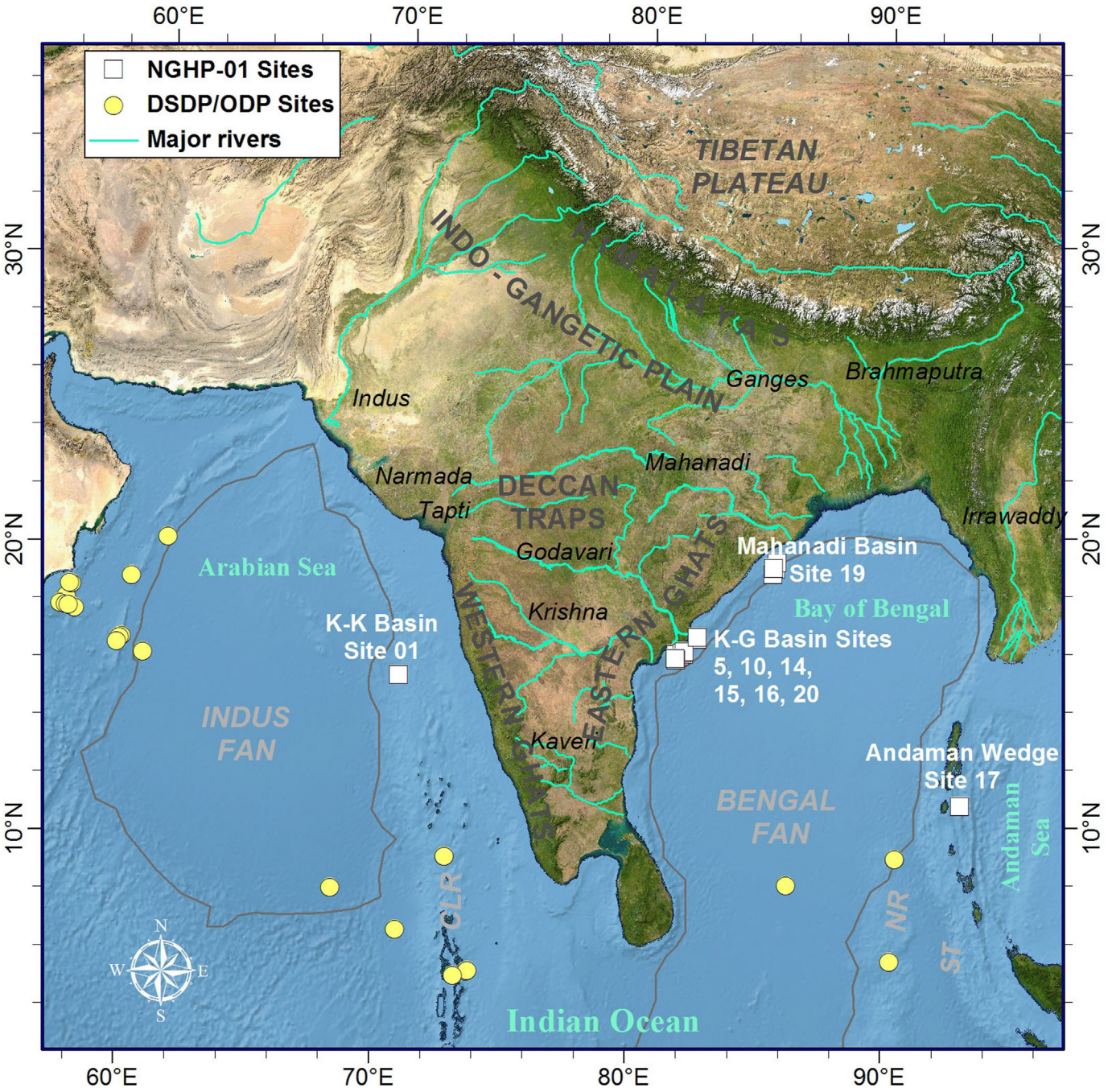


**Figure 1.** Regional map showing the locations of scientific drill and core sites throughout the northern Indian Ocean region. Labeled NGHP01 sites were sampled for the analyses in this study. CLR (Chagos-Laccadive Ridge), NR (Ninetyeast Ridge), and ST (Sunda Trench).

grabens that have accumulated 4–7 km of Late Carboniferous to recent sediments in the K–G basin (Bastia and Nayak, 2006) and up to 4 km of Cretaceous to recent sediments in the Mahanadi basin (Nyak and Rao, 2002). The sediments deposited in the offshore K–G basin are sourced from the Krishna and Godavari Rivers (Fig. 1), which drain the Deccan Basalts and deliver suspended sediment loads rich in smectite with minor feldspar, quartz, kaolinite, and illite (Subramanian, 1980; Phillips et al., 2014). Slumping, debris flows, and turbidites are common within the offshore K–G basin (Collett et al., 2008; Ramprasad et al., 2011; Shanmugam et al., 2009). Sediments recovered during NGHP01 at Krishna–Godavari sites are hemipelagic clays containing minor abundances of calcareous nannofossils and foraminifera, silt/sand lamina/beds, authigenic carbonates (Teichert et al., 2014), and iron sulfides (Collett et al., 2008). There is widespread evidence for gas hydrate from seismic profiles within the K–G basin (Jaiswal et al., 2012; Ramana et al., 2009), and gas hydrate was recovered and/or inferred in multiple holes in this basin during NGHP-01 coring and logging (Collet et al., 2008; Lee and Collett, 2009; Riedel et al., 2011; Shankar and Riedel, 2011) and was often present in fractures (Cook and Goldberg, 2008; Rees et al., 2011). Poor calcareous nannofossil and foraminfera preservation within the K–G basin cores limited biostratigraphic age determinations beyond a few datums that indicate the recovered sediments within the K–G basin are most likely Quaternary (~1.5 Ma) to recent in age (Flores et al., 2014).

Sediments deposited in the offshore Mahanadi Basin are sourced primarily from the Mahanadi River (Fig. 1) that drains the eastern Deccan traps and the Precambrian Eastern Ghat province (Rickers et al., 2001). Kaolinite, chlorite, quartz, dolomite, and minor montmorillonite and illite are characteristic suspended sediments discharged by the Mahanadi to the Bay of Bengal (Chakrapani and Subramanian, 1990; Subramanian, 1980; Phillips et al., 2014a). Sediments recovered by NGHP-01 in the Mahanadi Basin are hemipelagic clays often bearing nannofossils or foraminifers (Collett et al., 2008; Phillips et al., 2014b). Well-developed bottom simulating reflectors (BSR's) in the Mahanadi Basin suggest gas hydrate potential (Collett et al., 2008; Prakash et al., 2010). In the NGHP-01 cores from the Mahanadi basin, diffuse gas hydrates were inferred from infrared (IR) temperature and $Cl^-$ anomalies, and high gas saturations in pressure cores (Collett et al., 2008). Additional shallow penetrating cores (up to 40 mbsf) near the NGHP-01 cores sites also document shallow (10–20 mbsf) sulfate–methane transitions zones, active AOM (anaerobic oxidation of methane), and microbial origins for the gases (Mazumdar et al., 2014) above the deeper gas hydrate bearing intervals observed in the NGHP-01 cores (Collett et al., 2008). Nannofossil biostratigraphy at NGHP01 Site 19 shows the recovered sediments are Late Miocene (~9 Ma) to recent in age (Flores et al., 2014).

### 2.2. Andaman Sea

Oblique subduction of the Indian Plate beneath the Sunda Plate since the Cretaceous created the Andaman accretionary wedge, forearc basin, volcanic arc and, back-arc basin (Pedersen et al., 2010; Cochran, 2010; Raju et al., 2007; Curry, 2005; Pal et al., 2003; Karig et al., 2001; Moore et al., 1980; Rodolfo, 1969). The Andaman Sea overlies the oblique spreading back-arc basin, which initiated during the Late Miocene time (Khan and Chakraborty, 2005; Raju et al., 2004). Forearc crustal scale strike-slip faults (primarily the West Andaman and Sagaing Faults in the north, and the Sumatran fault to the south) accommodate much of the oblique plate motion and back-arc seafloor spreading (Martin et al., 2014; Cochran, 2010; Raju et al., 2007; Nielsen et al., 2004). The Andaman Sea is isolated from the Bengal and Nicobar submarine fans by the uplifted, accretionary wedge and Andaman Islands (Moeremans et al., 2013; Curry et al., 2002).

Within the Andaman Sea, surface sediment samples show terrestrial organic matter in sediments from the Irrawaddy River is deposited on the shelf, north of the Andaman back-arc spreading center (Ramaswamy et al., 2008). This distribution is consistent with (Rodolfo, 1975) who suggested ~90% of the total sediment load from the modern Irrawady is restricted to the nearshore region by monsoonal surface currents. Site NGHP-01-17 is located in the Andaman accretionary wedge, east of Little Andaman Island (Fig. 1) at a depth of 1344 m. This depth is well above the reach of sediment gravity flows associated with the Bengal Fan or Irrawady Delta and thus allowed the Site NGHP-01-17 location to preserve a nearly continuous record of pelagic/hemipelagic sedimentation. Sediments recovered at Hole NGHP-01-17A are comprised of calcareous nannofossil oozes with varying amount of foraminifera and siliceous microfossils and volcanic ash beds (Collett et al., 2008; Cawthern et al., 2014; Rose et al., 2014). Clay mineralogy at Site NGHP-01-17 is dominated by the smectite group (Phillips et al., 2014a) consistent with other observations of smectite-rich sediments along the Sunda Arc (Kolla and Biscaye, 1973). Gas hydrate accumulations were predominantly in volcanic ashes below ~250 mbsf at Site NGHP-01-17 due to enhanced secondary porosity from authigenic carbonate mineralization (Rose et al, 2014). Calcareous nannofossil biostratigraphy at Site NGHP-01-17A shows the recovered sediments are Late Miocene (~9 Ma) to recent (Flores et al., 2014).

### 2.3. Kerala Konkan Basin

The Kerala–Konkan (K–K) Basin is located on the western margin of peninsular India (Fig. 1). The western continental margin of India formed during two rifting events associated with the break-up of the Gondwana supercontinent during the Mesozoic (Kalaswad et al., 1993; Royer et al., 2002). The first was the rifting of India and the Seychelles from Madagascar in the Late Cretaceous (~84 Ma) (Royer et al., 2002; Schlich, 1981). The second was the rifting between the Seychelles and India near the Cretaceous–Tertiary boundary (~65 Ma), which was accompanied by the extensive volcanism of the Deccan flood basalts (Collier et al., 2008; Courtillot et al., 1988; Duncan and Pyle, 1988). The northward motion of the Indian plate due to seafloor spreading in the Arabian Sea and continental collision with the Eurasian plate created uplift and subsequent erosion of the Himalayas, western Tibet, and the Karakoram. The large flux of sediments eroded from these ranges led to the development of the Indus Fan (Clift et al., 2001) in the Arabian sea and the Bengal Fan (Curry et al., 2002) in the Bay of Bengal, the two largest submarine fans on Earth. The Chagos-Laccadive Ridge is a prominent N–S trending aseismic ridge offshore western India that most likely represents a hotspot track that evolved from past spreading ridge and Reunion hotspot volcanism (Duncan and Pyle, 1988; Fisk et al., 1989). Western peninsular India has a well-defined escarpment, the Western Ghats or Sahyadri, running parallel to the coast for 1500 km at an average height of 1200 m (Campanile et al., 2008). The Western Ghats form the drainage divide for peninsular India. The present pattern of precipitation over southern peninsular India clearly shows that monsoonal rains in western India fall preferentially on the strip of land between the coast and the Ghats highlands under an orographic influence (Xie et al., 2006).

The K–K Basin is the southernmost sedimentary basin offshore western India and it receives its sediments primarily from the adjacent Western Ghats range (Campanile et al., 2008). Between the Chagos-Laccadive Ridge and the western margin of

Indian almost all of the river discharge from western peninsular India is retained on the shelf; less than 5% is deposited in the deeper parts of the basin (Ramaswamy et al., 1991). Hole NGHP-01-01A is located at a depth of 2663 m in the distal part of the basin, just north of the Chagos-Laccadive Ridge and it contains a pelagic record of sedimentation. The sedimentary sequence in Hole NGHP-01-01A is dominated by calcareous oozes (Collet et al., 2008). The clay mineralogy at Hole NGHP-01-01A is dominated by illite (Phillips et al., 2014a) and is consistent with the observation of elevated illite content along the continental slope on the western Indian margin from transport of weathered metamorphic rocks of peninsular India, Indus Fan sediments along the slope, as well as Bay of Bengal sediments transported around Peninsular India (Chauhan and Gujar, 1996; Kessarkar et al., 2003; Rao and Rao, 1995). Calcareous nannofossil biostratigraphy at Site 01A shows a continuous record of sedimentation since the Oligocene (~33 Ma) (Flores et al., 2014). No gas hydrate or indications of gas hydrate were present at this site (Collett et al., 2008).

## 3. Methods

### 3.1. CHN elemental analysis

K–G Basin Holes NGHP-01-05D, NGHP-01-15A, NGHP-01-16A, Mahanadi Basin Hole NGHP-01-19A, and Andaman Sea Hole NGHP-01-17A were measured at a resolution of one sample per core section (1.5 m). K–G Basin Holes NGHP-01-5C, NGHP-01-10B, NGHP-01-10D, NGHP-01-14A, NGHP-01-20A, NGHP-01-20B, and K–K Basin Hole NGHP-01-01A were measured at a resolution of one per core (9.5 m). All sediment samples were refrigerated at 4 °C after collection to prevent decomposition of organic material. Approximately 5 $cm^3$ of bulk sediment sample was sub-sampled for carbon and nitrogen analysis. Samples were transferred to a shell vial and dried for 1–3 days at 40 °C. Upon drying, samples were crushed using an agate mortar and pestle and then stored in a desiccator.

Prior to TOC analysis inorganic carbon (IC) was dissolved using 6% sulfurous acid applied to weighed samples (e.g. Jablonski et al., 2002; Verardo et al., 1990) in amounts and steps optimized for carbonate-rich sediments (Phillips et al., 2011). Carbon and nitrogen in the sediments were measured using the Perkin Elmer CHN 2400 Series II CHNS/O Analyzer. C/N ratios were calculated using the wt. % TOC and TN, and their respective atomic weights. $CaCO_3$ weight percents were calculated by multiplying the IC weight percents (IC = TC-TOC) by 8.33 to account for the non-carbon mass fraction. The calculated bulk $CaCO_3$ fraction represents biogenic, authigenic, and any detrital carbonate phases. Repeatability error was established by analyzing replicate samples and calculating the standard deviation. Duplicate samples were run approximately every 10 samples by depth. Potential outliers were also run in duplicate.

### 3.2. Isotopic analysis

A subset of samples analyzed for CHN analysis were measured for $\delta^{13}$TOC using elemental analysis-isotope ratio-mass spectrometry (EA-IR-MS) on a Thermo Finnegan Delta Plus XP mass spectrometer interfaced to a Costech ECS 4010 Elemental Analyzer. 30–50 mg of powdered sample was acidified to remove IC using the same method as our CHN analysis (Phillips et al., 2011). Isotopic ratios are reported relative to the Vienna Pee Dee Belemnite (‰ VPDB). Duplicate samples were measured every ten samples.

## 4. Results

A total of 682 samples were analyzed separately for TC, TOC, IC, TN, and C/N. These included six holes within the K–G Basin: NGHP-01-15A, NGHP-01-16A, NGHP-01-05C, NGHP-01-10B, NGHP-01-10D, NGHP-01-14A, NGHP-01-20A and NGHP-01-20B and one hole each was analyzed in the Mahanadi (NGHP-01-19A), K–K Basin (NGHP-01-01A), and Andaman Sea (NGHP-01-17A). Isotopic measurements of TOC were completed for K–G Basin Holes NGHP-01-16A, NGHP-01-10B and NGHP-01-10D, Mahanadi Basin Hole NGHP-01-19A, Andaman Sea Hole NGHP-01-17A, and K–K Basin Hole NGHP-01-01A. These results are summarized below and shown in Figures 2–13 and Tables 1 and 2.

### 4.1. Krishna–Godavari Basin

At Hole NGHP-01-15A TC is dominated by the TOC fraction. The most prominent aspect of the down-core variation is a broad increase and decrease of TOC that ranges the entire hole (Fig. 2). TOC increases from 1.28% at 28 mbsf to a maximum of 3.18% at 87 mbsf (not including a wood-containing sample consisting of 10.17% TOC also at 87 m) and then decreases to 0.87% at the maximum depth of 197 mbsf. There is an additional enhancement of TOC between 10 and 27 m depth. The C/N is consistently greater than 10 suggesting the influence of soil organic matter (SOM) and vascular land plants on TOC. The shape of the C/N profile downcore, roughly mirrors the TOC pattern, except for an increased variance in C/N between 10 and 50 m. $CaCO_3$ is consistently low (less than 10%) throughout much of Hole NGHP-01-15A; however there is an anomalous increase at 20 mbsf, where $CaCO_3$ reaches 30 wt. %.

Hole NGHP-01-16A can be partitioned into four different intervals based on TOC content (Fig. 3). TOC is high and variable (mean = 1.92, standard deviation ($\sigma$) = 0.37) from 0 to 32 mbsf, lower and more consistent between 32 and 72 mbsf (mean = 0.95, $\sigma$ = 0.25), moderate and variable (mean = 1.53, $\sigma$ = 0.33) between 72 and 114 m, and moderate and consistent (mean = 1.32, $\sigma$ = 0.15) between 125 and 218 mbsf. The transition between the first two segments is abrupt, while the other two transitions are indistinct due to gaps in core recovery. C/N ratios follow the TOC pattern closely, except in the upper 32 mbsf where C/N is relatively constant while TOC is highly variable. Below 108 mbsf, $\delta^{13}$TOC is consistently between −13 and −14‰ VPDB. $\delta^{13}$TOC becomes more depleted between 108 and 68 mbsf, and above 51 mbsf. $CaCO_3$ is less than 15 wt. % for most of the record, with the exception of the interval 9–15 mbsf, where $CaCO_3$ reaches 23 wt. %.

Holes NGHP-01-10B and -10D has TOC content ranging between 0.6 and 2.4 wt. % and the TOC drives the downcore TC pattern (Fig. 4). TOC gradually increases with depth, punctuated by decreases below 1 wt. % at 92 and 144 mbsf and abrupt increases in TOC at 129 and 188 mbsf. C/N ratios are between 7 and 17 from 0 to 61 mbsf and between 2 and 11 below 61 mbsf. $\delta^{13}$TOC at Site 10B/D increased from −19.8 to −13.5‰ VPDB between 189 and 101 mbsf, then decreases to −19.3‰ VPDB at 61.9 mbsf. Above 61.9 mbsf., $\delta^{13}$TOC increases to 15.4‰ VPDB then decreases to −17.7‰ VPDB at 1.91 mbsf. $CaCO_3$ content generally varies between 3 and 8 wt. %, with several increases to greater than 10 wt. % between 91.2 and 144.4 mbsf.

At Hole NGHP-01-14A TOC ranges between 1.27 and 2.35 wt. % above 86.85 mbsf, and between 0.84 and 1.80 below 86.85 mbsf (Fig. 5). Similar to the pattern in TOC, C/N is higher (11.5–22.7) above 107.12 msbf, and lower below (6.7–14.3). For most of the record at NGHP-01-14A, $CaCO_3$ content is below 10 wt. % and

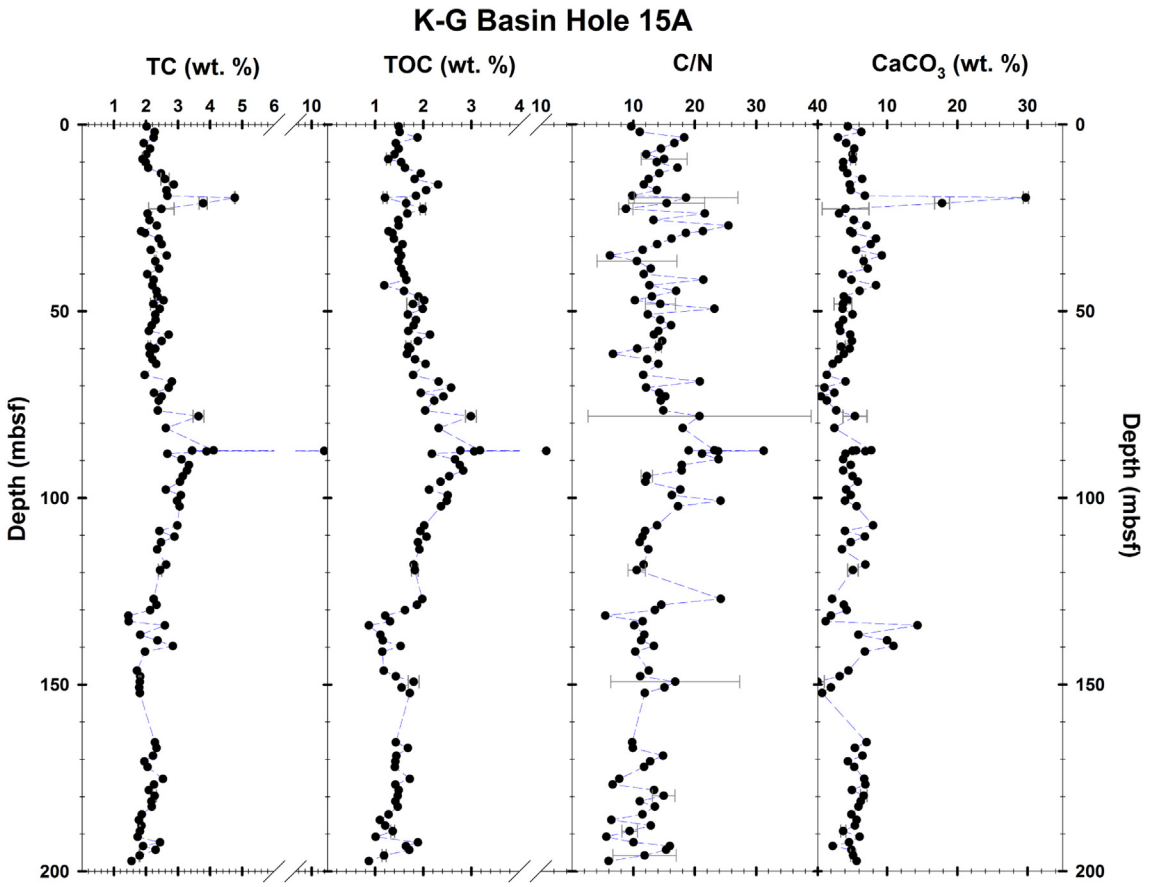


**Figure 2.** Results from Hole NGHP01-15A. The four panels, from left to right, display TC (total carbon), TOC (total organic carbon), C/N (TOC/Total N), and $CaCO_3$. Error bars represent the 2 standard deviation error of duplicate samples.

decreases with depth. One sample at 3.6 mbsf contains 13.7 wt. % $CaCO_3$.

At Holes NGHP-01-05C and -05D TOC varies between 0.59 and 2.32 wt. % (Fig. 6). High-resolution sampling in the upper 35 mbsf (Hole NGHP-01-05D) show high variability and little overall trend with depth. Low-resolution sampling to 178 mbsf (Hole NGHP-01-05C) show variation within the range of the upper interval and a slight increase with depth. C/N follows a similar trend with C/N ranging between 5 and 30, with most samples between 10 and 20. $CaCO_3$ is less than 5 wt. % for most of the record except for an increased interval as high as 29.4 wt. % between 12 and 35 mbsf.

At Hole NGHP-01-20A and -20B TOC is highly variable ranging from 0.65 wt. % to 2.2 wt.% with highest TOC content between 42 and 94 mbsf (Fig. 6). The downcore pattern in C/N ranges from 5 to 30, a range almost identical to the record at Hole NGHP-01-05C. $CaCO_3$ at Hole NGHP-01-20A and -20B is below 6 wt. % for most of the record, with increases to between 7 and 10 wt. % at 20.2, 94.2, and 123.52 mbsf.

### 4.2. Mahanadi Basin

At Hole NGHP-01-19A in the Mahanadi Basin TC (total carbon) variation is controlled by both $CaCO_3$ and TOC (Fig. 7). Most TOC values are between 0.9 and 1.3. wt. %, with intervals of enhanced and more variable TOC (1.5–2.2 wt. %) in the upper 30 m, between 70 and 110 m, and 200–250 m. TOC exhibits repeated increases and decreases with average variation of 0.22 wt. % between adjacent samples. C/N is generally greater than 10 and

**Table 1**
TOC, C/N, and $CaCO_3$ summary statistics for sites in the K–G basin. Table includes the number or samples ($n$), mean, standard deviation ($\sigma$), and 95% confidence intervals for each site and the K–G basin combined.

| | **TOC (wt. %)** | | | |
|---|---|---|---|---|
| **Site** | ***n*** | **Mean** | ***σ*** | **95%C.I.** |
| 05C/D | 42 | 1.66 | 0.38 | 0.12 |
| 10B/D | 31 | 1.50 | 0.34 | 0.12 |
| 14A | 19 | 1.53 | 0.38 | 0.17 |
| 15A | 113 | 1.84 | 0.92 | 0.17 |
| 16A | 125 | 1.36 | 0.41 | 0.07 |
| 20A | 20 | 1.56 | 0.39 | 0.17 |
| All K–G | 350 | 1.58 | 0.64 | 0.07 |
| | **C/N** | | | |
| **Hole** | ***n*** | **Mean** | ***σ*** | **95%C.I.** |
| 05C/D | 42 | 14.2 | 1.90 | 0.57 |
| 10B/D | 31 | 8.56 | 3.93 | 1.40 |
| 14A | 19 | 14.8 | 4.09 | 1.84 |
| 15A | 113 | 14.1 | 4.59 | 0.85 |
| 16A | 125 | 11.6 | 1.60 | 0.28 |
| 20A | 20 | 15.7 | 6.26 | 2.89 |
| All K–G | 347 | 12.90 | 3.97 | 0.42 |
| | **$CaCO_3$ (wt. %)** | | | |
| **Hole** | ***n*** | **Mean** | ***σ*** | **95%C.I.** |
| 05C/D | 42 | 7.15 | 6.42 | 1.94 |
| 10B/D | 31 | 6.49 | 3.83 | 1.35 |
| 14A | 19 | 5.77 | 2.73 | 1.23 |
| 15A | 113 | 5.22 | 3.37 | 0.62 |
| 16A | 125 | 5.92 | 3.39 | 0.59 |
| 20A | 20 | 5.60 | 3.10 | 1.36 |
| All K–G | 350 | 5.87 | 3.89 | 0.41 |

the upper 100 m exhibits increased and highly variable C/N. Similar to TOC, C/N exhibits variable increases and decreases at an interval at or less than the sampling interval. $\delta^{13}$TOC is variable in the upper 80 mbsf, varying between −20.9 and −16.8‰ VPDB. Below 80 mbsf, $\delta^{13}$TOC decreases from −20.0 to −21.9‰ VPDB. $CaCO_3$ is enhanced in the upper 80 mbsf and diminished in the lower sections of the hole. Above 80 mbsf, $CaCO_3$ varies from 2 to 42 wt. % in a recurring pattern. Below 80 mbsf, $CaCO_3$ increases with depth from 0.5 wt. % to 9 wt%.

### 4.3. Andaman Sea

At Hole NGHP-01-17A TC variability is largely attributed to the $CaCO_3$ content with intervals of augmented TOC generally less than 1 wt. % (Fig. 8). $CaCO_3$ follows a pattern with high content in the top 80 mbsf, decreased $CaCO_3$ between 80 and 200 mbsf, increased $CaCO_3$ over the interval 200 to 500 mbsf, and then decreased $CaCO_3$ 500 mbsf to the bottom of the core. TOC decreases over the upper 28 mbsf, increases from 28 to 87 mbsf, decreases from 87 to 187 mbsf, and then increases from 187 mbsf to the bottom of the hole. The majority of samples at NGHP-01-17A, exhibit C/N ratios less than 10 (mean 6.31) that are typical of those of marine plankton with only minor terrestrial organic carbon contributions. C/N variation is correlated with TOC content. $\delta^{13}$TOC decreases from the top of the hole (−20.1‰ VPDB) to 340 mbsf, (−22.4‰ VPDB) with short-term variability on the order of 1‰ VPDB. $\delta^{13}$TOC increases to −20.8‰ VPDB at 503 mbsf and then decreases to the bottom of the hole.

### 4.4. Kerala–Konkan Basin

At Hole NGHP-01-01A in the Konkan Basin TC is a dominated by the high $CaCO_3$ (10–88 wt.%) and very low TOC (0.04–0.68 wt. %) measured at this site (Fig. 9). $CaCO_3$ decreases from 40 to 22 wt. % in the top 150 mbsf, then increases dramatically (from 22 to 86 wt. %) from 150 to 287 mbsf, reaching over 80% $CaCO_3$. TOC decreases with depth to less than 0.1 wt. % below 188 mbsf. C/N ratios follow a comparable trend to TOC and all measurements are within the range of marine plankton, but trend toward minor terrestrial input at shallower depths. C/N ratios below 200 mbsf is below the range expected for marine organic matter. $\delta^{13}$TOC increases from the bottom of the hole (−26.8‰ VPDB) to 126 mbsf (−20.2‰ VPDB) and remains between −20.2 and −18.8‰ VPDB above 126 mbsf.

**Table 2**
TOC, C/N, and $CaCO_3$ summary statistics comparing K–G basin, Mahanadi Basin, Andaman Sea, and Konkan Basin. Table includes the number or samples (n), mean, standard deviation (σ), and 95% confidence intervals for each site and the K–G basin combined.

| | **TOC (wt. %)** | | | |
|---|---|---|---|---|
| **Hole** | ***n*** | **Mean** | ***σ*** | **95%C.I.** |
| K–G | 350 | 1.58 | 0.64 | 0.07 |
| 19A | 188 | 1.12 | 0.22 | 0.03 |
| 17A | 418 | 0.73 | 0.22 | 0.02 |
| 01A | 30 | 0.27 | 0.17 | 0.06 |
| | **C/N ratio** | | | |
| **Hole** | ***n*** | **Mean** | ***σ*** | **95%C.I.** |
| K–G | 347 | 12.9 | 3.97 | 0.42 |
| 19A | 184 | 11.1 | 2.29 | 0.33 |
| 17A | 418 | 6.49 | 2.05 | 0.20 |
| 01A | 30 | 4.01 | 2.98 | 1.07 |
| | **$CaCO_3$ (wt. %)** | | | |
| **Hole** | ***n*** | **Mean** | ***σ*** | **95%C.I.** |
| K–G | 350 | 5.87 | 3.89 | 0.41 |
| 19A | 188 | 4.54 | 4.80 | 0.69 |
| 17A | 418 | 29.4 | 6.98 | 0.67 |
| 01A | 30 | 43.8 | 21.7 | 7.77 |

### 4.5. Cross Site comparison

Significant differences in TOC content (wt. %) and source (inferred from C/N and $\delta^{13}$TOC) and $CaCO_3$ content (wt %) exist

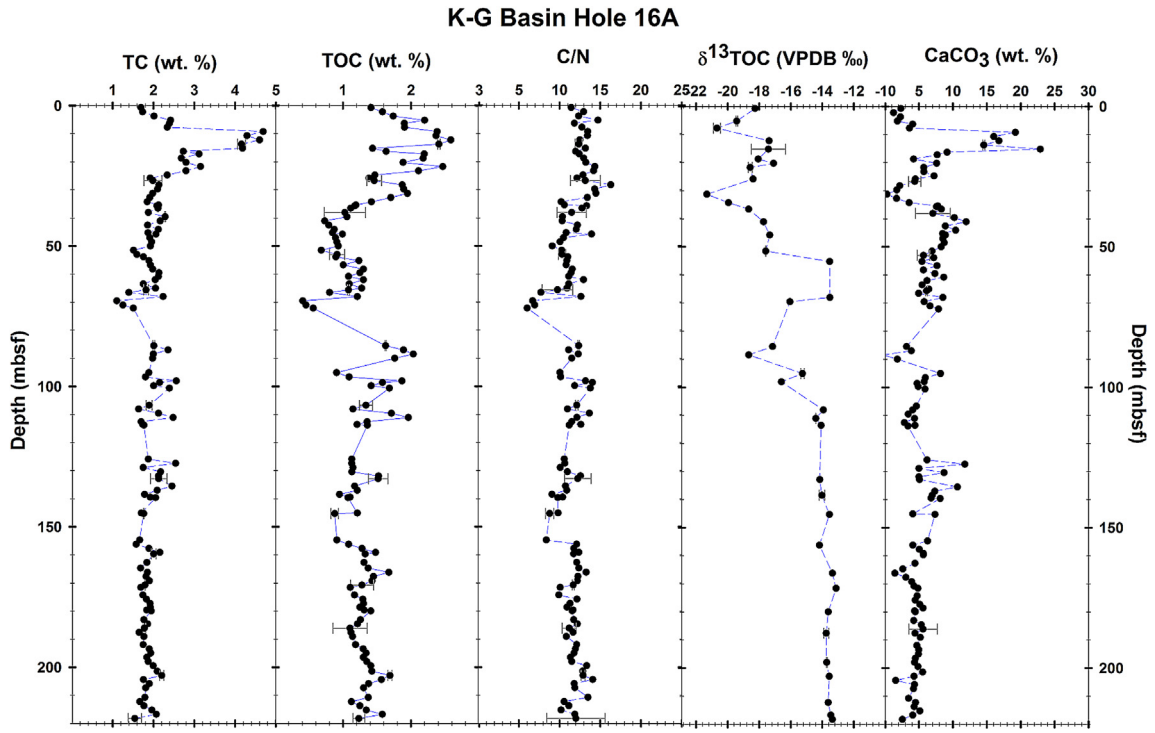


**Figure 3.** Results from Hole NGHP01-16A. The five panels, from left to right, display TC (total carbon), TOC (total organic carbon), C/N (TOC/total N), $\delta^{13}$TOC, and $CaCO_3$. Error bars represent the 2 standard deviation error of duplicate samples.

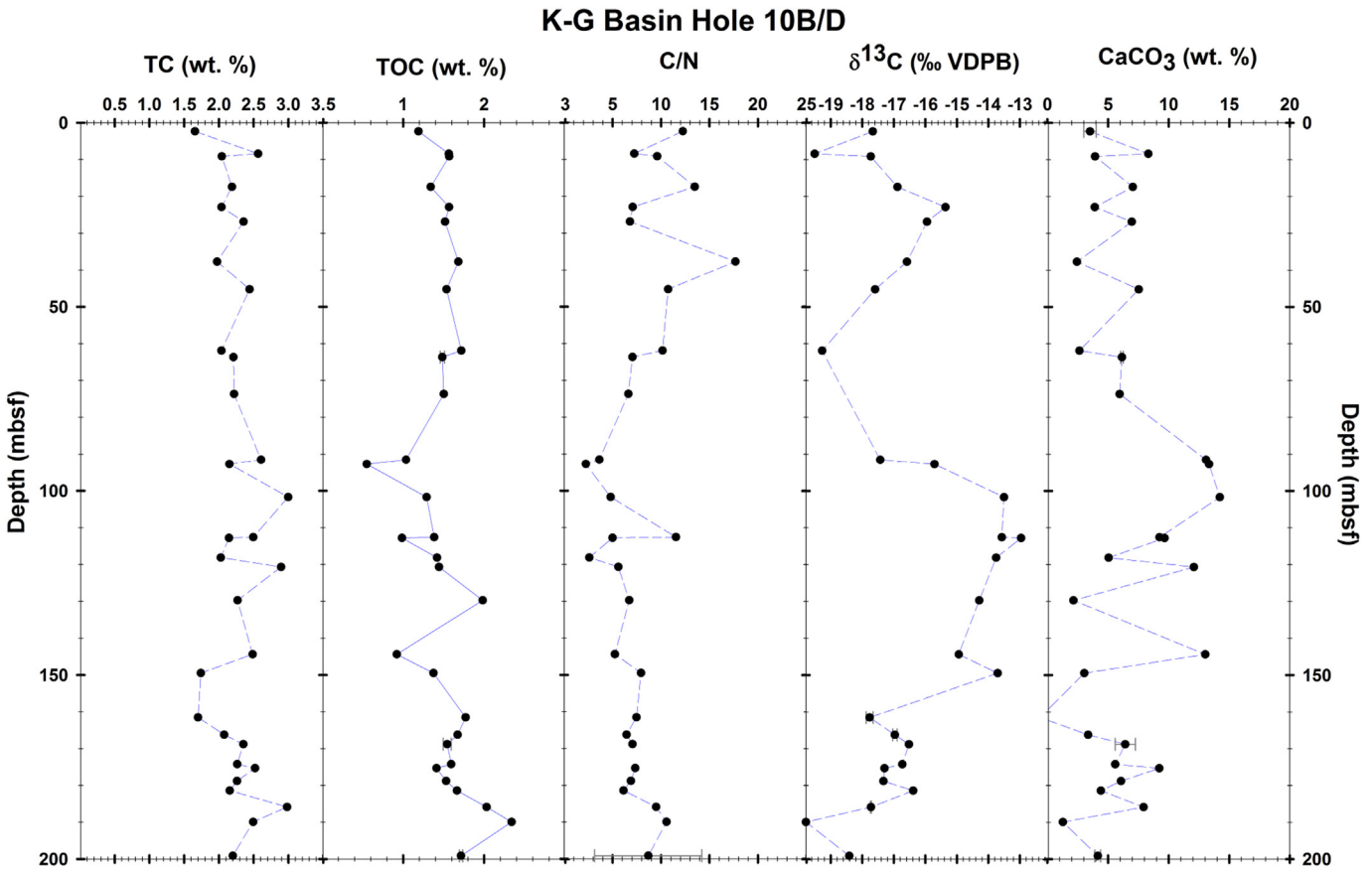


**Figure 4.** Results from Hole NGHP01-10B/D. The five panels, from left to right, display TC (total carbon), TOC (total organic carbon), C/N (TOC/total N), $\delta^{13}$TOC, and $CaCO_3$. Error bars represent the 2 standard deviation error of duplicate samples.

between the holes cored during the NGHP-01 Expedition. TOC content (wt. %) is similar across the Krishna–Godavari Basin (Fig. 10, Table 1) and between the Krishna–Godavari Basin holes and Mahanadi Basin Hole NGHP-01-19A (Fig. 11, Table 2). Andaman wedge Hole NGHP-01-17A and K–K Basin Hole NGHP-01-01A have distinctly lower TOC content than the Mahanadi or K–G Basin sites (Fig. 11, Table 2). Within the K–G Basin, mean TOC content ranges from 1.36 to 1.84 wt. % (Fig. 10, Table 1). Statistically significant differences exist in mean TOC between Hole NGHP-01-16A with the lowest TOC wt. % in the K–G Basin and Hole NGHP-01-15A with highest TOC wt. % in K–G Basin (Table 1). No significant differences in mean TOC exist between any other K–G sites. All sites in the K–G basin have similarly low values of $CaCO_3$; however the sites sampled at a high-resolution (Holes NGHP-01-05D, -15A, and -16A) show periodic increases in carbonate in the upper 50 m.

Mean TOC (1.58 wt. %) from all the K–G Basin sites combined decreases to Hole NGHP-01-19A (1.12 wt. %), Site 17A (0.73 wt. %), and Site 01A (0.27 wt. %) (Fig. 11, Table 2). Differences between these locations are significant shown by 95% confidence intervals. Similarly to trends in TOC, C/N decreases from K–G Basin sites (12.9) to Hole NGHP-01-19A (11.1), Hole NGHP-01-17A (6.49), and Hole NGHP-01-01A (4.01) (Table 2). C/N is relatively consistent at K–G Basin sites except Site NGHP-01-10 which is lower (Table 1). $CaCO_3$ is similarly low at K–G Basin sites (5.87 wt. %) and Hole NGHP-01-19A (4.43 wt.%) compared to the much higher mean $CaCO_3$ wt % at both Hole NGHP-01-17A (29.4 wt. %) and Hole NGHP-01-01A (43.8 wt.%) (Table 2).

Between Sites (K–G, Mahanadi, Andaman, K–K) $\delta^{13}$TOC values vary and range between −28 and −12‰ VPDB (Fig. 12). When plotted with C/N, these values represent a range of TOC sources that trends between marine and $C_4$ plant material at Holes NGHP-01-10B, -10D, -16A, and -19A (Fig. 12). TOC at Hole NGHP-01-17A is within the range expected for marine organic matter. At Hole NGHP-01-01A, samples above 200 mbsf fall within the C/N and $\delta^{13}$CTOC (formatted correctly) range of marine organic matter, while samples below 200 mbsf have C/N less than marine organic matter and $\delta^{13}$CTOC (again format please) consistent with $C_3$ organic matter (Fig. 12). The trend in $\delta^{13}$TOC and C/N is also apparent in site averages, and site averaged $\delta^{13}$TOC increases with increasing TOC content and decreasing $CaCO_3$ content; C/N also decreases with increasing $CaCO_3$ content (Fig. 13).

## 5. Discussion

### 5.1. Regional variation in TOC and $CaCO_3$

The mean TOC content in the recovered cores is greatest in the K–G Basin and progressively decreases to the Mahanadi Basin (Hole NGHP-01-19A), the Andaman wedge (Hole NGHP-01-17A), and K–K Basin (Hole NGHP-01-01A) (Table 2). This pattern is generally consistent with the sedimentation rates, which decrease in the same order (K–G sed rates 12.5–48 cm/1000 yr; Mahanadi 1–13 cm/1000yr, Andaman wedge 5–13 cm/1000 yr; K–K Basin 0.4–2.5 cm/1000 yr; Flores et al., 2014). Under oxic bottom water conditions higher sedimentation rates result in efficient carbon burial, thus higher TOC contents in the marine sediments (Müller and Suess, 1979; Stein, 1990). The recovered sedimentology of the cores and the geologic setting in each region is also consistent

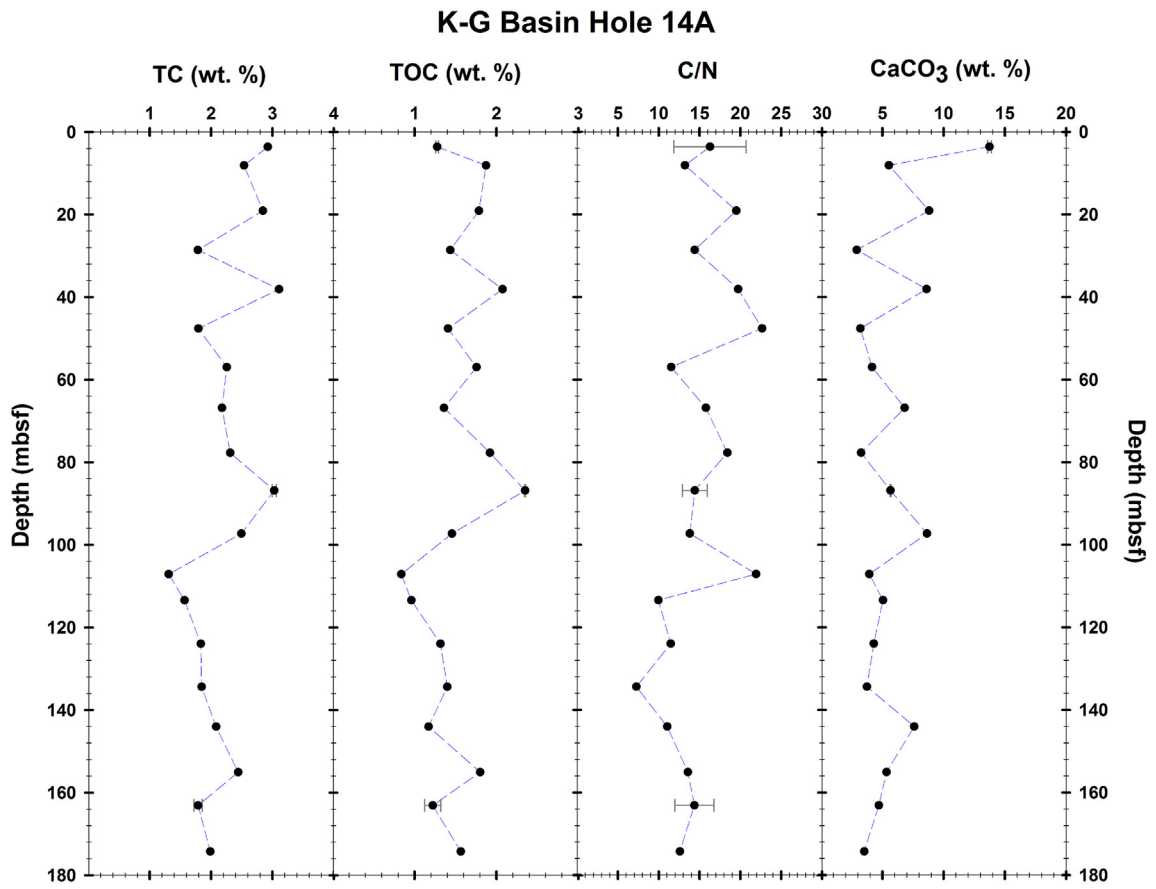


**Figure 5.** Results from Hole NGHP01-14A. The four panels, from left to right, display TC (total carbon), TOC (total organic carbon), C/N (TOC/total N), and $CaCO_3$. Error bars represent the 2 standard deviation error of duplicate samples.

with this pattern. The highest sedimentation rates and TOC contents in the K–G Basin cores correspond with the presence of silt and sand turbidites and with visible organic carbon detritus. These materials are derived from the proximal Krishna and Godavari River deltas and transported across the narrow continental shelf to the NHGP-01 core sites (Collett et al., 2008). The high flux of terrigenous fluvial material at these sites significantly dilutes the marine biogenic components in the records, making calcareous nannofossil and foraminifera biostratigraphy difficult (Flores et al., 2014). These high sedimentation rates also restrict the recovery of sediments older than Quaternary in the ~200–300 m long cores recovered across the basin. The cores recovered from the Mahanadi basin to the north, are finer grained (Collett et al., 2008), due to their location distal to the Mahanadi river outflow, which results in a lower hemipelagic sedimentation rate. The sediment composition at Hole NGHP-01-19A reflects both distal lithogenic (clay) and biogenic (calcareous and siliceous) sedimentation (Collett et al., 2008). Hole NGHP-01-17A in the Andaman wedge is far from the lithogenic fluvial discharge of the Irrawady River and thus records a pelagic record of predominantly carbonate ooze with biosiliceous rich intervals (Cawthern et al, 2014) and abundant volcanic ashes (Collett et al., 2008; Rose et al, 2014). The equivalent basal age of the Hole NGHP-01-17A and Hole NGHP-01-19A records, despite their thickness differences, may reflect the addition of volcanic ashes to the Hole NGHP-01-17A stratigraphy, which has thickened the equivalent time section here (691 m long core) compared to Hole NGHP-01-19A (305 m long core). The very slow sedimentation rate at Hole NGHP-01-01A reflects its distal position relative to the fluvial discharges from the Western Ghats coupled with a location on the continental slope above the Indus fan. The sediments at Hole NGHP-01-01A are carbonate oozes, reflecting biogenic-rich pelagic sedimentation with low lithogenous input in the Arabian Sea since the Oligocene at this site; these low rates of accumulation result in the much poorer preservation of organic carbon at this site.

Regional variation in $CaCO_3$ content (Table 2) across the four study regions, shows the highest $CaCO_3$ occurs at the most pelagic, biogenic sediment dominated sites, NGHP-01-01A and -17A. Mean $CaCO_3$ is slightly higher in the K–G basin, however, than at the Mahanadi basin, even though calcareous biogenic sediment constituents are more abundant at Site NGHP-01-19 (Collett et al., 2008). This difference can be explained by the presence of abundant authigenic carbonates throughout the K–G basin stratigraphy (Teichert et al., 2014, Collett et al., 2008; Mazumdar et al., 2009). Our measurement of the bulk total carbon and total organic carbon to derive the bulk $CaCO_3$ includes not only biogenic carbonate microfossils, but also any authigenic or detrital carbonate present in the sediments. The influence of authigenic carbonate on the $CaCO_3$ content in the K–G Basin is more pronounced due to the low amount of biogenic carbonate preserved in the record. In the Mahanadi, Andaman, and K–K basins authigenic carbonates are significantly less abundant (Collett et al., 2008), but the overwhelming amount of biogenic carbonate at these sites makes any additional contribution from authigenic carbonate to the bulk $CaCO_3$ likely minor, but difficult to assess. No detrital carbonate phases were identified in smear slides or coarse fractions described at sea at any of the NGHP-01 sites (Collett et al., 2008).

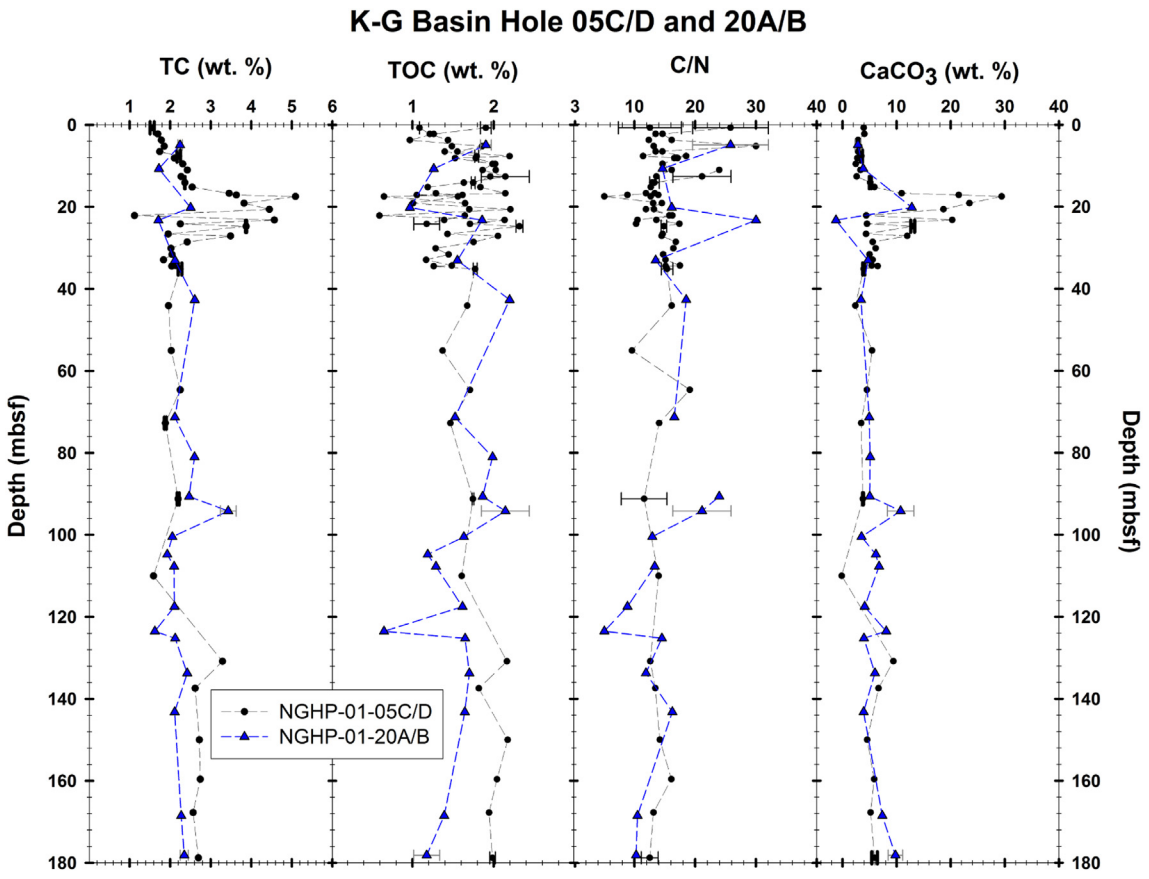


**Figure 6.** Results from Hole NGHP01-05C, -05D, and -20A. The four panels, from left to right, display TC (total carbon), TOC (total organic carbon), C/N (TOC/total N), and $CaCO_3$. Error bars represent the 2 standard deviation error of duplicate samples.

### 5.2. Regional variation in $\delta^{13}C_{TOC}$ and C/N

Variations in organic carbon sources are evident from $\delta^{13}C_{TOC}$ and C/N measurements and show a similar trend across the four study regions. The $\delta^{13}C_{TOC}$ and C/N cross-plot of these parameters show a trend between a terrestrial end-member with C/N > 12 and $\delta^{13}C_{TOC}$ > −17‰ and a marine end-member with C/N of approximately 5 and $\delta^{13}C_{TOC}$ of approximately −20‰ (Fig. 13). The TOC at K–G Basin Holes NGHP-01-10B/D and -16A are predominantly terrestrial, Mahanadi Basin Hole NGHP-01-19A is likely a mix of terrestrial and marine carbon, and Hole NGHP-01-17A in the Andaman Wedge and Hole NGHP-01-01A in the K–K basin are predominantly marine (Fig. 12). A contribution from $C_4$ plant carbon can explain the $\delta^{13}C_{TOC}$ values greater than −20‰ that comprise most of the records at K-G Basin Holes NGHP-01-10B/D, -16A, and Mahanadi Hole 19A (Fig. 13). The $C_4$ plant contribution to the Bay of Bengal has been significant since the Miocene, as shown by an increase in $\delta^{13}C_{TOC}$ from −24 to −27‰ to-15 to −24‰ at 7 Ma in Bengal Fan sediments (France-Lanord and Derry, 1994; Freeman and Colarusso, 2001). In the Quaternary records at Hole NGHP-01-16A and −10B/D in the K–G Basin downcore shifts in $\delta^{13}C_{TOC}$ from −21 to −13 (Figs. 3 and 4) and relatively constant C/N are consistent with the equivalent shift in $\delta^{13}C_{TOC}$ observed on glacial–interglacial timescales in the Mahanadi basin from companion Hole NGHP-01-19B (Phillips et al., 2014) and in the upper 70 m of Hole NGHP-01-19A (Fig. 7). Cores from the Bengal Fan also document this dramatic change in $\delta^{13}C_{TOC}$ during the last 19 Ka (Galy et al., 2008). Significant changes in the source vegetation in the interior of the Indian peninsula due to monsoon variability occuring during the Holocene have also been documented by measurements of the isotopic composition of strictly terrestrial leaf waxes at Site NGHP-01-16 (Ponton et al., 2012) At orbital timescales, higher resolution and better age constrained studies of Phillips et al. (2014b) and Galy et al. (2008) suggest a shift in source vegetation that was $C_4$ dominant during glacial periods and $C_3$ dominant during interglacials, and is consistent with vegetation modeling that suggests drier conditions during glacial intervals and wetter conditions during interglacials driven by variations in the strength of the summer and winter monsoon. This glacial-interglacial $\delta^{13}C_{TOC}$ pattern is also observed in the western Arabian Sea, eastern Bay of Bengal, and Andaman Sea (Fontugne and Duplessy, 1986) and consistent with the 84 to 18 ka record of $\delta^{13}C$ in soil organic carbon and carbonates in the Ganga Plain observed by Agrawal et al. (2012).

In the longer late Miocene to recent records at Sites NGHP-01-19 and -17, downcore variation in $\delta^{13}C_{TOC}$ is only observed at Site 19, where it varies from −17 at the top of the record to −22 at the base of the record (Fig. 7) with a nearly constant C/N range between 10 and 12 (Fig. 7). This shift over a longer timescale is consistent with the onset of $C_4$ plant deposition on the Bengal Fan at 7 Ma (France-Lanord and Derry, 1994; Freeman and Colarusso, 2001). Our $\delta^{13}C_{TOC}$ data at Site NGHP-01-19 suggests the increase in $C_4$ plant flux relative to $C_3$ plants to the Bay of Bengal at 7 Ma was not just from the Ganges-Bramaputra drainage, but from the peninsular Indian Mahanadi river drainage as well. Over the same time interval as Site NGHP-01-19 the $\delta^{13}C_{TOC}$ at Site 17 in the Andaman wedge is far less variable

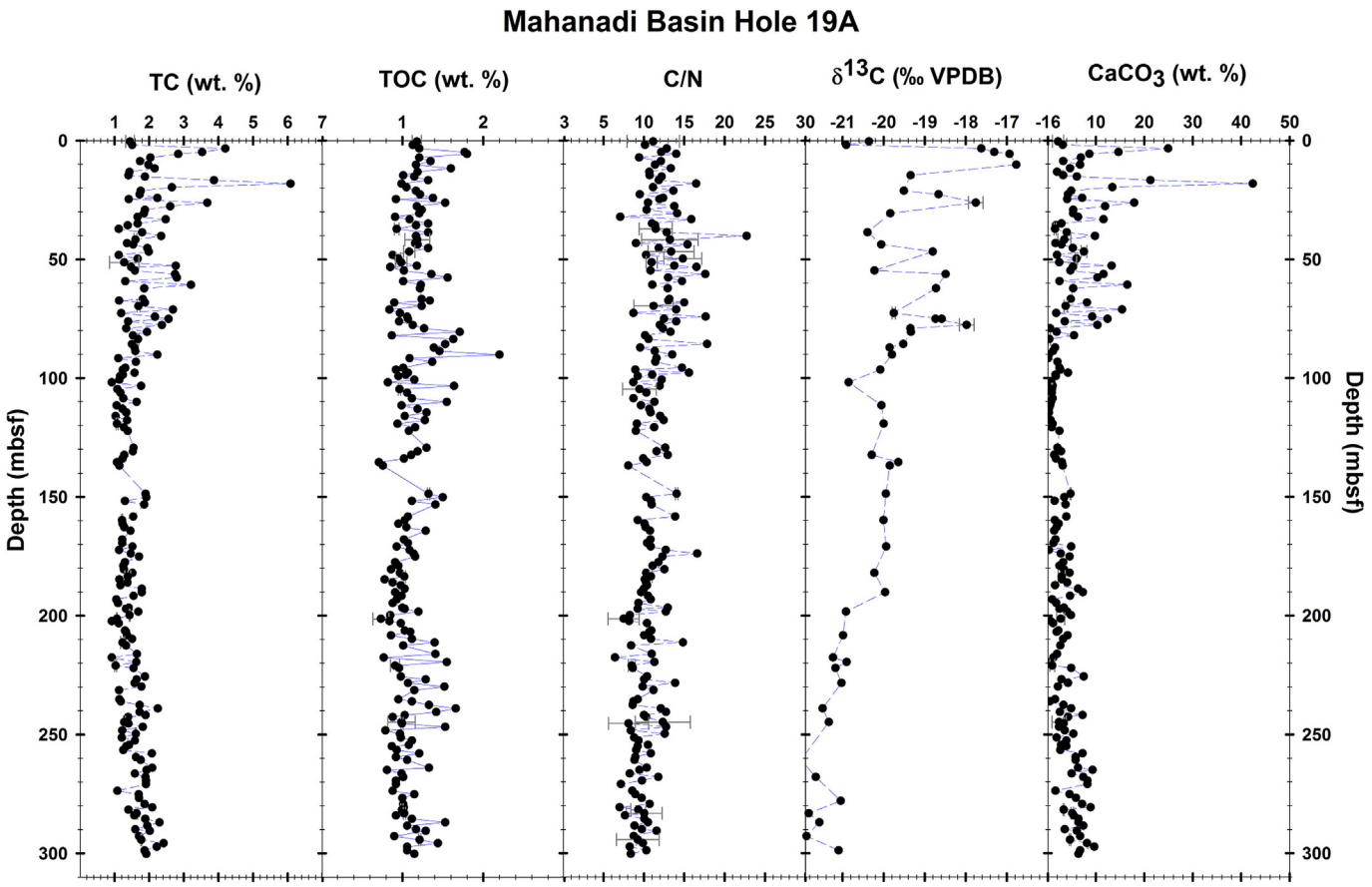


**Figure 7.** Results from Hole NGHP01-19A. The five panels, from left to right, display TC (total carbon), TOC (total organic carbon), C/N (TOC/total N), $\delta^{13}$TOC, and $CaCO_3$. Error bars represent the 2 standard deviation error of duplicate samples.

(Fig. 8). At Site NGHP-01-17 both the C/N and $\delta^{13}C_{TOC}$ are consistent downcore and represent a predominance of marine organic carbon (Fig. 12), which is consistent with the carbonate and siliceous bearing carbonate oozes observed throughout the records. In the late Oligocene to recent record at Hole NGHP-01-01A in the K–K Basin, the $\delta^{13}C_{TOC}$ and C/N show a dramatic shift in the record (Fig. 9) likely reflecting a shift from $C_3$ plants to increased marine or $C_4$ plant organic matter at 150 mbsf (approximately 18 Ma), marking a major change in the climate regime and/or depositional system.

### 5.3. Observed and inferred gas hydrate

During the NGHP-01 Expedition, gas hydrates were observed in recovered samples from conventional and pressurized cores and inferred from: (1) IR thermal anomalies produced by gas hydrate presence, (2) $Cl^-$ anomalies in pore water profiles, (3) soupy and moussy sediment textures produced by gas hydrate dissociation, and (4) resistivity increases from *in situ* borehole LWD (logging while drilling) or wireline resistivity measurements (Collett et al., 2008). From these NGHP-01 initial shipboard observations and measurements and post-cruise analyses gas hydrates are well-documented in the K–G and Mahanadi Basins, and in the Andaman wedge, but not observed in the K–K Basin (Table 3). The highest gas hydrate saturations occur throughout the K-G Basin, where most of the physical samples of gas hydrate were recovered. They occur predominantly in fractures at K–G Sites NGHP-01-10 and -05 (Table 3) (Collett et al., 2008; Cook and Goldberg, 2008; Lee and Collett, 2009; Riedel et al., 2010, Rees et al., 2011), but are also hosted within sand and silt horizons (Collett et al., 2008, Table 3). Downhole log based resistivity saturation estimates are known to overestimate gas hydrate saturations in fractured reservoirs (Collet et al., 2014), thus, Cl-based saturation estimates for K-G Basin sites (from Solomon et al., 2014) are also shown in Table 3 and for the fractured reservoirs may represent more realistic gas hydrate saturations. Lower gas hydrate saturations (~15%) were calculated at Hole NGHP-01-19A in the Mahanadi Basin in the ~25 m interval above the BSR (Table 3) and at 125–130 mbsf, where low-level IR thermal and Cl-anomalies and pressure core degassing results suggest the presence of disseminated gas hydrate (Collett et al., 2008). Gas hydrate saturations were calculated in excess of 50% in discreet ashes from ~250 mbsf to the BSR (608 mbsf) at Site NGHP-01-17 in the Andaman accretionary wedge (Collett et al., 2008; Rose et al., 2014; Table 3). These saturations are similar to those in the K–G basin and were also associated with IR thermal and $Cl^-$ anomalies and inferred from analyses of pressure cores (Collett et al., 2008). Gas hydrates or indicators of gas hydrate were not observed or detected in the K–K Basin (Collett et al., 2008).

### 5.4. TOC and gas hydrate

Comparison of the four regions cored and logged during the NGHP-01 expedition show a trend in mean TOC that decreases from the K–G Basin, Mahanadi, Andaman, and K–K basins (Fig. 11, Table 2). This pattern is consistent with the depositional environments and lithology (Collett et al., 2008) and sedimentation rates (Flores et al., 2014) in each region. Measurements of the bulk TOC in long, ocean drilling obtained sediment cores collected throughout

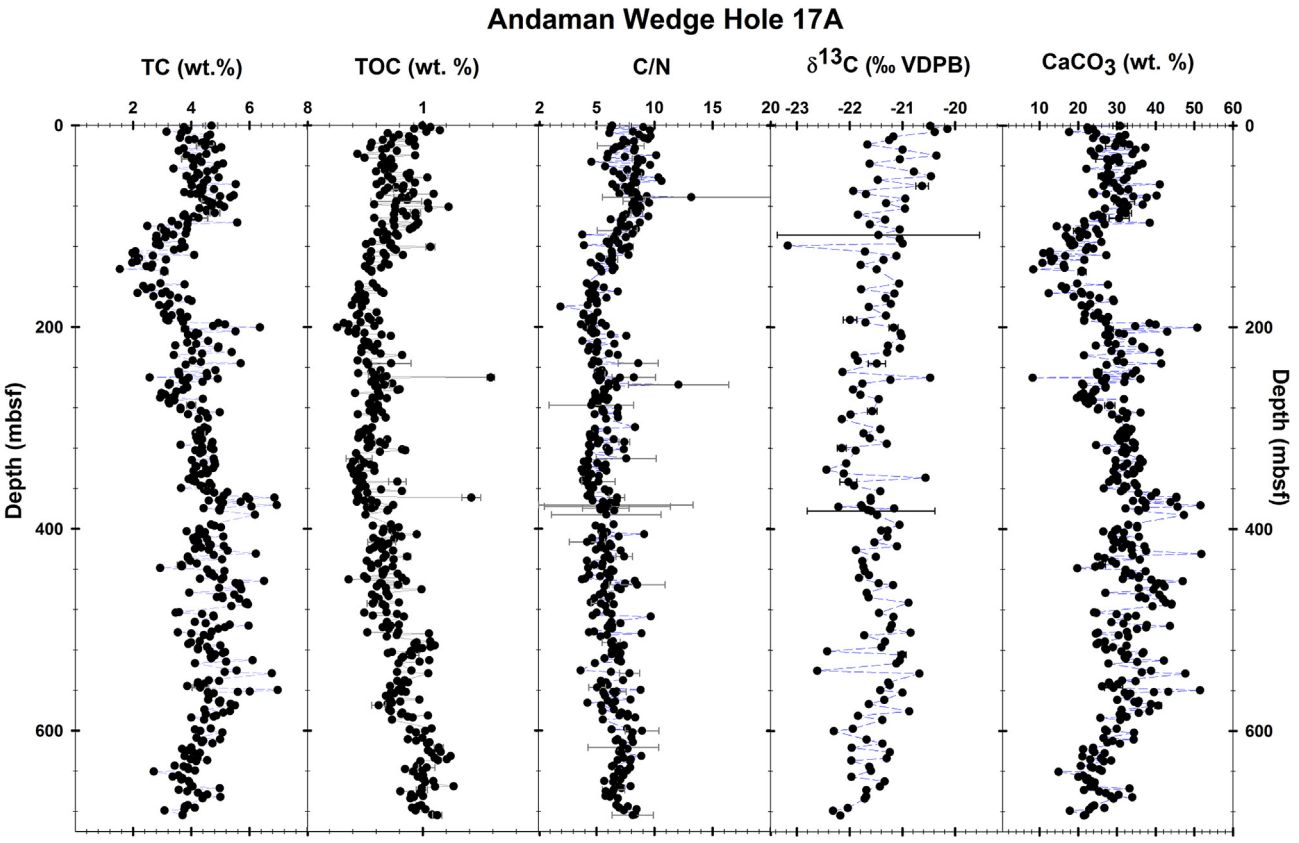


**Figure 8.** Results from Hole NGHP01-17A. The five panels, from left to right, display TC (total carbon), TOC (total organic carbon), C/N (TOC/total N), $\delta^{13}$TOC, and $CaCO_3$. Error bars represent the 2 standard deviation error of duplicate samples.

the gas hydrate stability zone can be indicative of the relative potential of a sedimentary sequence to generate methane *in situ* and may be characteristic of similar, deeper (*ex situ*) gas producing depositional systems in the subsurface. One way to examine the role of TOC on gas hydrate formation is to measure the microbial activity of methanogens in sediment core samples and the rates of methanogenesis in lab culturing experiments (e.g. Colwell et al., 2004). Lab culture experiments, however, typically overestimate methanogenic rates due to artificial microbial stimulation, making it difficult to assess a threshold value of TOC need to fuel enough methanogenesis to produce gas hydrate. Another approach is to use numerical models (e.g. Davie and Buffett, 2001; Archer et al., 2012; Archer and Buffett, 2012), including reactive transport models (e.g. Wallmann et al., 2012) to calculate gas hydrate saturations using multiple input parameters collected from ocean drilling cores (e.g. sedimentation rates, rates of methanogenesis, rates of organic carbon degradation, wt % TOC, porosity and permeability, etc.). These modeling approaches can work well to produce more realistic global gas hydrate estimates, but their intrinsic value is in the incremental improved understanding they provide about the major controlling factors that influence gas hydrate formation and accumulation in marine sediments. Wallmann et al. (2012), suggests that methane hydrate formation is basically controlled by the following key parameters: (1) accumulation of particulate organic carbon at the seafloor; (2) kinetics of microbial organic matter degradation and methane generation in marine sediments; (3) thickness of the GHSZ; (4) solubility of methane in pore fluids within the GHSZ; (5) sediment compaction; an (6) ascent of deep-seated pore fluids and methane gas into the GHSZ. Results from a two-dimensional numerical model for passive margin gas hydrate accumulation (Archer et al., 2012) suggest the abundance of methane hydrate responds strongly to changes in the degradation rate of organic matter, to gas transport and redissolution in the sediment column, and to ocean and subsurface temperatures. Important in both simulations is the role of TOC accumulation and degradation. There seems to be a consensus that 0.4 wt. % TOC (Klauda and Sandler, 2005) to 0.5 wt.% TOC (Waseda, 1998) is a realistic minimum amount of TOC needed to fuel enough methanogenesis to generate *in situ* gas hydrate at low (1–2%) saturations. Wallmann et al., 2012 suggest that gas hydrate saturations greater than 3% pore volume must be generated by advective delivery of methane from depth.

Once formed, however, the total amount of gas hydrate that accumulates is not only a function of the methane produced within or delivered to the GHSZ, but also the reservoir capacity of the sediments. Gas hydrate reservoirs exist in marine sediments as stratigraphic or fractured/faulted systems, both providing high porosity and permeability for gas hydrate growth and saturation of pore space. Whether the gas that forms the gas hydrate is produced *in situ* from methanogenesis of TOC within the gas hydrate stability zone (GHSZ) or advection of gas from deeper depths can be inferred from measurements of gas composition and isotopic signature (e.g. Whiticar, 1999). Many gas hydrate systems are predominantly microbial in origin, however, making it difficult to assess the relative roles of *in situ* vs *ex situ* methane production using gas measurements alone. Reaction transport models that incorporate a comprehensive set of concentration and isotopic data can also be used to help discriminate between *in situ* and *ex situ* methane sources (e.g. Hong et al., 2013, Hong et al., 2013a,b). In addition, examination of seismic reflection profiles, which provide evidence of structural traps, faults, gas chimneys, and fluid charged faults or stratigraphic conduits indicative of advective fluid flow,

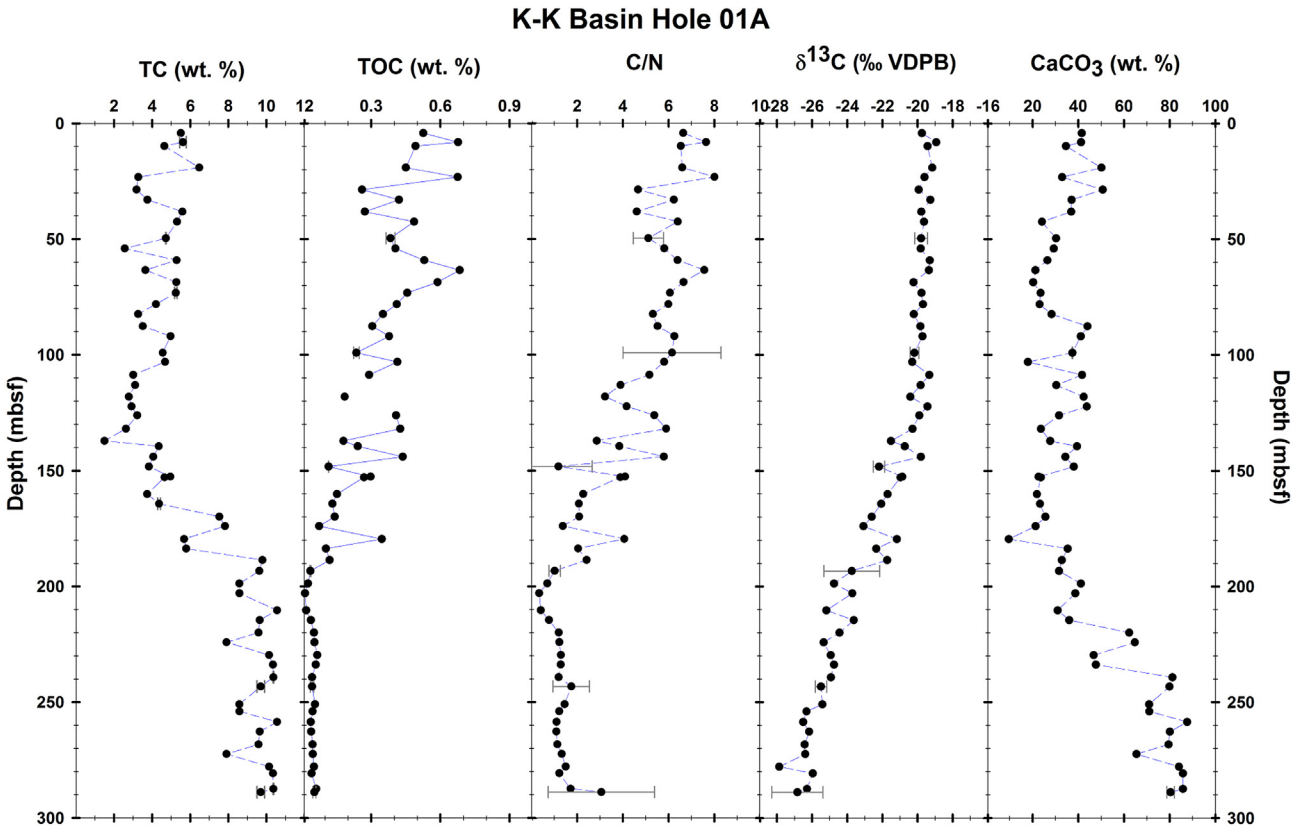


**Figure 9.** Results from Hole NGHP01-01A. The five panels, from left to right, display TC (total carbon), TOC (total organic carbon), C/N (TOC/total N), $\delta^{13}$TOC, and $CaCO_3$. Error bars represent the 2 standard deviation error of duplicate samples.

can also be used to assess the potential influence of *ex situ* produced gases in gas hydrate systems (e.g. Tréhu et al., 2004; Bünz et al., 2012).

In the four NGHP-01 study regions, the highest mean TOC contents occurred in the cores from the Krishna–Godavari Basin and these records also contain some of the highest observed maximum gas hydrate saturations (Table 3). Detailed seismic and geophysical logging studies and pressure core imaging document abundant fracture hosted gas hydrate in the K–G basin at Sites NGHP-01-5 and -10 (Collett et al., 2008; Cook and Goldberg, 2008; Lee and Collett, 2009; Riedel et al., 2010, Rees et al., 2011) and pore filling, stratigraphic hosted gas hydrate at the remaining sites (NGHP-01-14, -15, 16, and 20) examined in this study (Collett et al., 2008). Sites 6 and 7 in the K–G Basin, not included in our study, also show fracture hosted gas hydrate accumulations (Cook et al., 2014). Despite abundant TOC available for *in situ* methanogenesis and gas hydrate formation, the faulted, fractured, and deformed stratigraphy observed in the K–G basin (Collett et al., 2008; Riedel et al., 2010) coupled with fracture and pore filling gas hydrate in saturations at many sites >20% (Table 3), suggests that advective processes may be contributing to the supply of methane to the gas hydrates throughout the K–G Basin. Pore water data from sites NGHP-01-03, 05, and 14, however, show no evidence for fluid advection, alternatively, the gas hydrate saturations at these sites may be the result of higher rates of *in situ* organic matter degradation and methanogenesis related to high, non-steady state sedimentation rates across the K–G basin (Solomon et al., 2014). Collectively these observations point to a complex system where both sedimentation patterns controlling carbon metabolic pathways and structural considerations that impact the basin hydrology act together to generate the observed gas hydrate distributions in the K–G basin.

At Hole NGHP-01-19A in the Mahanadi basin, mean TOC content is less than at the K–G sites (Table 3), but still above the 0.4–0.5 wt% threshold for significant *in situ* methanogenesis and gas hydrate formation. Gas hydrate observed here was pore filling, stratigraphic hosted, and abundant TOC throughout the record is consistent with *in situ* methanogenesis. The relatively high maximum gas hydrate saturation attained at this site (20%), the presence of ethane, although microbial in origin and propane in the core (Collett et al., 2008), and the existence of thermogenic gases deeper in the basin (Raju and Sharma, 2006), however, suggests there may be some advection of deeper gases into the GHSZ. Interpretation of seismic reflection profiles in the vicinity of Site NGHP-01-19 by Shankar and Riedel (2014) suggest that faults may exist near the expected BSR and could serve as conduits for deeper gases to the GHSZ. Similar to the K–G basin, *ex situ* formed methane and in this case also ethane and propane, likely combine with *in situ* formed methane to produce gas saturations high enough to produce the observed gas hydrate at this site.

At Hole NGHP-01-17A in the Andaman wedge, mean TOC content is less than that at the Mahanadi basin (Table 3) and barely above the 0.4 to 0.5 wt. % threshold for significant *in situ* methanogenesis and gas hydrate formation. Yet, maximum gas hydrate saturations (up to 76%) exceed those observed at the Mahanadi basin and are comparable to those observed in the K–G basin. Gas compositions at Site NGHP-01-17 are dominated by methane, with minor microbial ethane and early thermogenic propane, consistent with a minor thermogenic component (Collet et al., 2008). Gas hydrates are pore filling in volcanic ashes at this

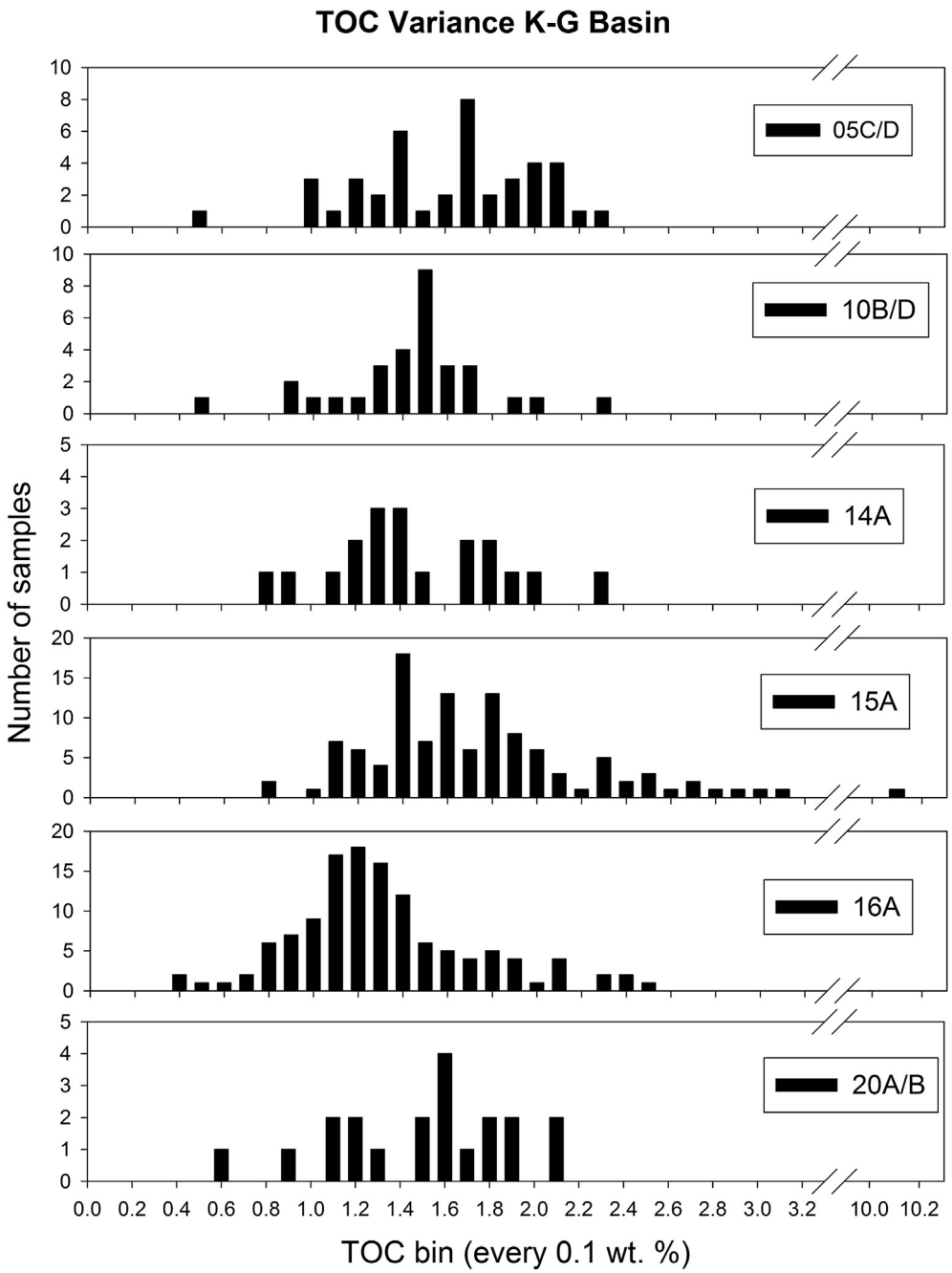


**Figure 10.** Histograms showing TOC distributions at Krishna–Godavari Holes NGHP01-05C, -05C, -10B, -10D, -14A, -15A, -16A, and -20A. Bin size for TOC is 0.1wt. %.

site (Rose et al., 2014) and site survey seismic data (Collett et al., 2008) show an extremely thick (~600 m) GHSZ within the folded accretionary wedge sediments. Seismic reflectors dip upward toward Site NGHP-01-17 as well and could provide pathways for gas migration from depth into and within the thick gas hydrate stability zone (Collett et al., 2008). Although some methane may be formed from *in situ* methanogenesis at this site, a significant fraction could be sourced from depth and advected up and into the GHSZ. High gas hydrate saturations here are also enabled by the enhanced porosity and permeability afforded by the volcanic ashes and by extreme porosity preservation, driven by authigenic carbonate precipitation, within the deeper stratigraphy (Rose et al., 2014).

The lowest mean TOC content (0.27 wt.%) was observed at Hole NGHP-01-01A in the K–K basin (Table 3). This amount of TOC is lower than the 0.4–0.5 wt. % TOC threshold for significant gas hydrate accumulation. No gas hydrate or evidence for gas hydrate was discovered at this site and furthermore, organic geochemical studies at Hole NGHP-01-01A were unable to detect any hydrocarbon gases (Collett et al., 2008). In addition, the apparent BSR at Hole NGHP-01-01A does not show reverse polarity compared to the seafloor, thus this seismic reflector is not gas hydrate related, but instead results from a sharp density contrast in the sediments (Collett et al., 2008). We suggest the low TOC content of the sediments at Hole NGHP-01-01A likely prohibits significant gas and gas hydrate formation at this site.

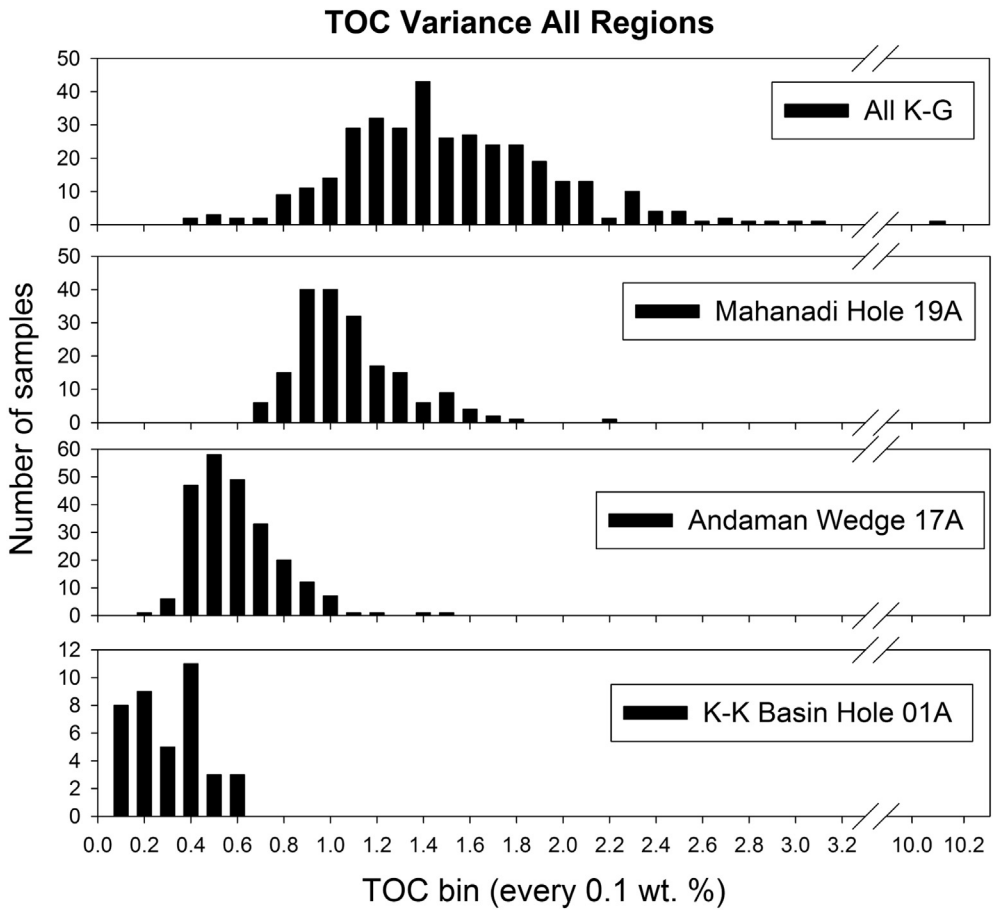


**Figure 11.** Histograms showing TOC distributions in the Krishna–Godavari Basin (all sites combined), Mahanadi Basin (Hole NGHP01-19A), Andaman Wedge (Hole NGHP01-17A), and K–K Basin (Hole NGHP01-01A).

*In situ* methanogenesis in the K–G and Mahanadi Basins and in the Andaman wedge is sustained by the preservation of sufficient TOC in these sedimentary records. Although our carbon isotope data suggest the K–G Basin records are sourced from potentially less labile terrestrial organic matter, the dynamic nature of sedimentation in the K–G basin, characterized by pervasive MTDs (Hong et al., 2014) greatly decreases the amount of time TOC spends in the sulfate reduction zone and enhances delivery of labile TOC to the methanogenic zone (Solomon et al., 2014). In the Mahanadi Basin, a mixed source of marine and terrestrial organic carbon coupled with a lower sedimentation rate results in less TOC preservation than the K–G basin sites, but still above the 0.4 to 0.5 wt. % threshold for significant methane production. In the Andaman wedge, our carbon isotope data suggest a marine origin for the organic carbon, but again the low sedimentation rate likely limits TOC preservation at this site to just above the 0.4 to 0.5 wt.% threshold. Consistent with the observations of Pohlman et al. (2009), data from the Indian continental margin shows that it is not the amount, but the exposure time of organic carbon on the seafloor (a function of sedimentation rate) that ultimately results in the preservation of significant TOC to fuel methanogenesis and form *in situ* gas hydrate. In non-advective gas hydrate systems, it is possible gas hydrate could be found under a range of TOC conditions in the sediments if sedimentation rates are high and carbon sources remain bioavailable (labile) below the sulfate reduction zone (e.g. Pohlman et al., 2009; Solomon et al., 2014; Hong et al., 2014). Superimposed on processes that result in *in situ* methane production is the strong role that folding and faulting play in the advective delivery of *ex situ* gases to the GHSZ. In the K–G and Mahanadi Basins and Andaman wedge the advection of gases may also contribute to the amount of gas hydrate observed and inferred in these regions.

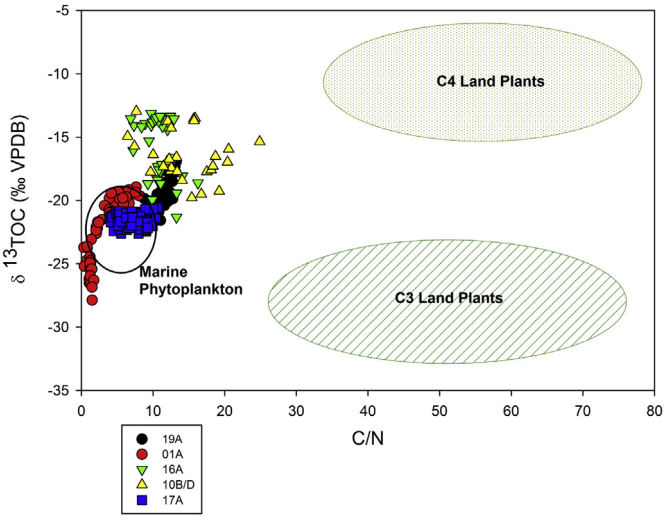


**Figure 12.** Scatterplot of all data measured for C/N and $\delta^{13}$TOC shown by site. Typical ranges in C/N and $\delta^{13}$TOC for marine plankton, $C_3$ plants, and $C_4$ plants is shown, after Meyers, 1994.

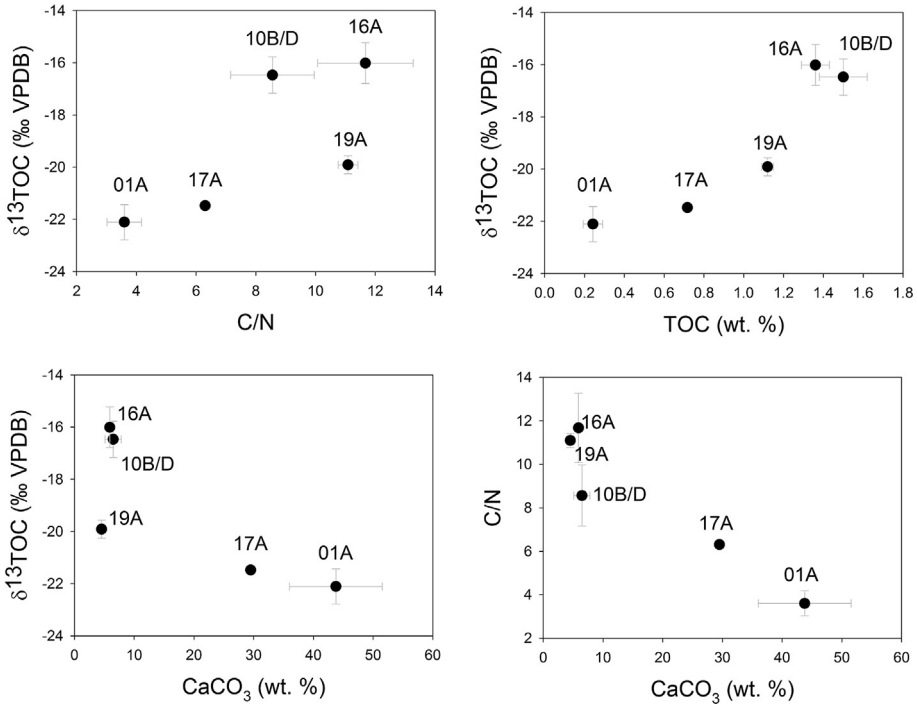


**Figure 13.** Cross-plots of TOC, $\delta^{13}$TOC, C/N, and $CaCO_3$ using averages from Holes NGHP-01-01A, -10B, -10D, -16A, -17A, -19A.

## 6. Conclusions

High organic carbon fluxes driven by marine productivity and/or terrestrial fluxes from fluvial sources and high sedimentation rates are conducive to high TOC preservation in marine sediments. Mean TOC abundance is greatest in the K–G Basin and decreases progressively to the Mahanadi basin, Andaman wedge, and K–K basin. This decrease in TOC is matched by a progressive increase in biogenic $CaCO_3$ and increasing distance from terrestrial sources of organic matter and lithogenic materials. Organic carbon sources span from terrestrial (K–G Basin) to mixed marine and terrestrial (Mahanadi Basin), to marine dominant (Andaman wedge and K–K basin) across the study areas. High rates of sedimentation in the K–G basin are driven by the close proximity of the Krishna and Godavari river deltas to the slope, across a narrow eastern peninsular Indian margin. A more distal location between the Mahanadi River and the Mahanadi basin site results in finer grained deposition and a lower sedimentation rate. The Andaman wedge site, is located distal from fluvial sources, and the pelagic sedimentation rate here is larger due to the addition of air fall volcanic ashes. Pelagic sedimentation in the K–K basin occurs at an even slower rate and fluvial sources are minimal and distal to this core site. In the K–G Basin, variation in the bulk $\delta^{13}C_{TOC}$ is consistent with changes in $C_3$ and $C_4$ vegetation driven by monsoon variability on glacial–interglacial timescales. In the Mahanadi Basin a shift in the $\delta^{13}C_{TOC}$ is similar to that observed on

**Table 3**
Summary of gas hydrate related characteristics (from Collett et al., this vol) with Mean TOC at each of the NGHP-01 sites examined in this study.

| NGHP-01 Hole | BSR depth (mbsf) | Log-based gas hydrate saturations[a] | $Cl^-$-based gas hydrate saturations[b] | Gas hydrate reservoir type[d] | Mean TOC wt. % |
|---|---|---|---|---|---|
| **K–G Basin** | | | | | |
| 05C/D | 125 | 20–70% | 2.3–13.4% | F–F with possible P–F | 1.66 |
| 10B/D | 160 | 50–85% | 1.5–41.3% | F–F with possible P–F | 1.50 |
| 14A | 109 | <20% | 0.9–15.5% | Possible P–F (highly dissem. gas hydrate) | 1.53 |
| 15A | 126 | 25–50% | 1.4–67.8% | P–F (ranging from dissem. to one highly saturated gas hydrate sand bed) | 1.84 |
| 16A | 170 | 25–50% | 1.1–12.7% | Possible P–F (dissem. gas hydrate) | 1.36 |
| 20A | 220 | N/A[c] | Not available | Possible P–F (dissem. gas hydrate) | 1.56 |
| **Mahanadi Basin** | | | | | |
| 19A | 205 | 5–20% | Not available | Possible P–F | 1.12 |
| **Andaman Wedge** | | | | | |
| 17A | 608 | 5–40% | <1–76% | P–F (ranging from dissem. to highly saturated gas hydrate in ash beds) | 0.73 |
| **K–K Basin** | | | | | |
| 01A | No BSR | No gas hydrate | No gas hydrate | N/A | 0.27 |

[a] Based on Archie analysis of downhole resistivity logs (Collett et al., this vol.).
[b] Based on porewater chlorinity (from Solomon et al., 2014, except for Hole 17A from Collett et al., this vol.).
[c] No LWD or wireline tools were run at this site, but IR and $Cl^-$ anomalies suggest finely dispersed gas hydrate.
[d] F–F (fracture-filling), P–F (pore-filling).

the Bengal Fan, recording the onset of $C_4$ plant deposition in the late Miocene. A large shift the $\delta^{13}C_{TOC}$ in the K–K basin is consistent with a change from $C_3$ to $C_4$ dominated plants during the middle Miocene.

Along the Indian margins we observed a close relationship between TOC content and gas hydrate saturation, however, additional factors also influence gas hydrate accumulation. In the K–G basin, the amount of TOC that is delivered to the methanogenesis zone is favored by high, non-steady state sedimentation (Solomon et al., 2014). In addition, seismic, borehole log, pressure core, and gas composition data, coupled with relatively high observed gas hydrate saturations at some sites in the K–G, Mahanadi and Andaman regions, suggest that advective gas transport may also play a major role in the saturation of methane and the formation of gas hydrates. We conclude that even though TOC content may be a first-order indicator for gas hydrate potential, sedimentation patterns regulate the amount of TOC available for *in situ* methanogenesis and furthermore, the structural and stratigraphic geologic environment will most likely dictate where the greatest gas hydrate saturations will occur.

## Acknowledgments

The authors wish to thank those that contributed to the success of the National Gas Hydrate Program Expedition 01 (NGHP01). NGHP01 was planned and managed through collaboration between the Directorate General of Hydrocarbons (DGH) under the Ministry of Petroleum and Natural Gas (India), the U.S. Geological Survey (USGS), and the Consortium for Scientific Methane Hydrate Investigations (CSMHI) led by Overseas Drilling Limited (ODL) and FUGRO McClelland Marine Geosciences (FUGRO). The platform for the drilling operation was the research drill ship JOIDES Resolution, operated by ODL. Much of the drilling/coring equipment used was provided by the Integrated Ocean Drilling Program (IODP) through a loan agreement with the US National Science Foundation. Wireline pressure coring systems and supporting laboratories were provided by IODP/Texas A&M University (TAMU), FUGRO, USGS, U.S. Department of Energy (USDOE) and HYACINTH/GeoTek. Downhole logging operational and technical support was provided by Lamont-Doherty Earth Observatory (LDEO) of Columbia University. The financial support for the NGHP01, from the Oil Industry Development Board, Oil and Natural Gas Corporation Ltd., GAIL (India) Ltd. and Oil India Ltd. is gratefully acknowledged. We also acknowledge the support extended by all the participating organizations of the NGHP: MoP&NG, DGH, ONGC, GAIL, OIL, NIO, NIOT, and RIL. We greatly appreciate the efforts of the NGHP01 shipboard scientific party for the collection and initial interpretation of these cores. This research was funded by the Directorate General of Hydrocarbons (DGH) India and the U.S. Geological Survey (Contract # 07CRSA0708). M.E.T. acknowledges support from a fellowship from the Institute for Advanced Study (HWK), Delmenhorst, Germany. Additional thanks to Madison Myers, Misty Cawthern, and Kristen Bulpett for onshore preparation of samples for CHN analysis. We thank Andy Ouimette, and Eduardo Miranda for assistance with C isotopic measurements. Constructive comments and suggestions from John Pohlman and two anonymous reviewers greatly improved this manuscript.

## References

Agrawal, S., Sanyal, P., Sarkar, A., Jaiswal, M.K., Dutta, K., 2012. Variability of Indian monsoon rainfall over the past 100 ka and its implication for $C_3$-$C_4$ vegetational change. Quat. Res. 77, 159–170.

Archer, D.E., Buffett, B.A., 2012. A two-dimensional model of the methane cycle in a sedimentary accretionary wedge. Biogeosciences 9, 3323–3336. http://dx.doi.org/10.5194/bg-9-3323-2012.

Archer, D.E., Buffett, B.A., McGuire, P.C., 2012. A two-dimensional model of the passive coastal margin deep sedimentary carbon and methane cycles. Biogeosciences. 9, 1–20. http://dx.doi.org/10.5194/bg-9-1-2012.

Bastia, R., Nayak, P.K., July 2006. Tectonostratigraphy and depositional patterns in Krishna offshore Basin, Bay of Bengal. Lead. Edge 818–829.

Brooks, J.M., Kennicutt II, M.C., Fay, R.R., McDonald, T.J., Sassen, R., 27 July 1984. Thermogenic gas hydrates in the Gulf of Mexico. Science 225 (4660), 409–411. http://dx.doi.org/10.1126/science.225.4660.409.

Bünz, Stefan, Polyanov, Sergey, Vadakkepuliyambatta, Sunil, Consolaro, Chiara, Mienert, Jurgen, 2012. Active gas venting through hydrate-bearing sediments on the Vestnesa Ridge, offshore W-Svalbard. Mar. Geol. 332–334 http://dx.doi.org/10.1016/j.margeo.2012.09.012. ISSN 0025-3227.s 189-197.s.

Burdige, D.J., 2005. Burial of terrestrial organic matter in marine sediments: a re-assessment. Glob. Biogeochem. Cycles 19, GB4011. http://dx.doi.org/10.1029/2004GB002368.

Campanile, D., et al., 2008. Sedimentation record in the Konkan-Kerala Basin: implications for the evolution of the Western Ghats and the Western Indian passive margin. Basin Res. 20 (1), 3–22. http://dx.doi.org/10.1111/j.1365-2117.2007.00341.x.

Carson, B., Screaton, E.J., 1998. Fluid flow in accretionary prisms: evidence for focused, time-variable discharge. Rev. Geophys. 36, 329–351.

Cawthern, T., Johnson, J.E., Giosan, L., Flores, J.A., Rose, K., 2014. A Late Miocene–Early Pliocene biogenic silica crash in the Andaman Sea and Bay of Bengal: potential teleconnections to the Pacific. Mar. Pet. Geol. 58, 490–501.

Chakrapani, G.J., Subramanian, V., 1990. Preliminary studies on the geochemistry of the Mahanadi River basin, India. Chem. Geol. 81, 241–253.

Chauhan, O.S., Gujar, A.R., 1996. Surficial clay mineral distribution on the southwest continental margin of India: evidence of input from the Bay of Bengal. Cont. Shelf Res. 16, 321–333.

Claypool, G.E., Kvenvolden, K.A., 1983. Methane and other hydrocarbon gases in marine sediments. Annu. Rev. Earth Planet. Sci. 11, 299–327.

Clayton, C., 1992. Source volumetric of biogenic gas generation. In: Vially, R. (Ed.), Bacterial Gas. Editions Technip, Paris, pp. 191–204.

Clift, P.D., et al., 2001. Development of the Indus Fan and its significance for the erosional history of the Western Himalaya and Karakoram. Geol. Soc. Am. Bull. 113 (8), 1039–1051. http://dx.doi.org/10.1130/0016-7606(2001)113<1039:dotifa>2.0.co;2.

Cochran, J.R., 2010. Morphology and tectonics of the Andaman Forearc, northeastern Indian Ocean. Geophys. J. Int. 182, 631–651.

Colwell, F.S., Matsumoto, R., Reed, D., 2004. A review of the gas hydrates, geology, and biology of the Nankai Trough. Chem. Geol. 205, 391–404.

Collett, T.S., Johnson, A.H., Knapp, C.C., Boswell, R., 2009. Natural Gas hydrates: a review. In: Collett, T., Johnson, A., Knapp, C., Boswell, R. (Eds.), Natural Gas Hydrates—Energy Resource Potential and Associated Geologic Hazards, AAPG Memoir 89, pp. 146–219.

Collett, T.S., Riedel, M., Cochran, J.R., Boswell, R., Presley, J., Kumar, P., Sathe, A., Sethi, A., Lall, M., Sibal, V., NGHP Expedition 01 Scientists, 2008. National Gas Hydrate Program Expedition 01 Initial Reports. Directorate General of Hydrocarbons, New Delhi.

Collett, Timothy S., Boswell, Ray., Cochran, James R., Kumar, Pushpendra., Lall, Malcolm., Mazumdar, Aninda., Ramana, Mangipudi Venkata., Ramprasad, Tammisetti., Riedel, Michael., Sain, Kalachand., Sathe, Arun Vasant., Vishwanath, Krishna., NGHP Expedition 01 Scientific Party, Geologic implications of gas hydrates in the offshore of India: Results of the National Gas Hydrate Program Expedition 01. Mar. Pet. Geol., Available online 4 September 2014, ISSN 0264-8172, http://dx.doi.org/10.1016/j.marpetgeo.2014.07.021.

Collier, J.S., et al., 2008. Age of Seychelles–India break-up. Earth Planet. Sci. Lett. 272 (1–2), 264–277. http://dx.doi.org/10.1016/j.epsl.2008.04.045.

Cook, A.E., Goldberg, D., 2008. Extent of gas hydrate filled fracture planes: implications for in situ methanogenesis and resource potential. Geophys. Res. Lett. 35, L15302. http://dx.doi.org/10.1029/2008GL034587.

Cook, A.E., Goldberg, D.S., Malinverno, A., 2014. Natural gas hydrates occupying fractures: a focus on non-vent sites on the Indian continental margin and the northern Gulf of Mexico. J. Mar. Pet. Geol. 58, 278–291.

Courtillot, V., et al., 1988. Deccan flood basalts and the Cretaceaous-Tertiary boundary. Nat. Lond. 333, 843–846.

Curry, J.R., Emmel, F.J., Moore, D.G., 2002. The Bengal Fan: morphology, geometry, stratigraphy, history and processes. Mar. Pet. Geol. 19, 1191–1223.

Curry, J.R., 2005. Tectonics and history of the Andaman Sea region. J. Asian Earth Sci. 25, 187–232.

Davie, M.K., Buffett, B.A., 2001. A numerical model for the formation of gas hydrate below the seafloor. J. Geophys. Res. 106 (B1), 497–514. http://dx.doi.org/10.1029/2000JB900363.

Duncan, R.A., Pyle, D.G., 1988. Rapid eruption of the Deccan flood basalts at the Cretaceaous/Tertiary boundary. Nature 333, 841–843.

Fisk, M.R., et al., 1989. Reunion hotspot magma chemistry over the past 65 m.y.: results from Leg 115 of the Ocean Drilling Program. Geology 17, 934–937.

Flores, J.-A., Johnson, J.E., Mejía-Molina, A.E., Alvarez, M.C., Sierro, F.J., Singh, S.D., Mahanti, S., Giosan, L., 2014. Sedimentation rates from calcareous nannofossil and planktonic foraminifera biostratigraphy in the Andaman Sea, northern Bay of Bengal, and Eastern Arabian Sea. J. Mar. Pet. Geol. 58, 425–437.

Fontugne, M.R., Duplessy, J.-C., 1986. Variations of the monsoon regime during the Quaternary: evidence from carbon isotopic record of organic matter in north Indian Ocean sediment cores. Palaeogeogr. Palaeoclimatol. Paleoecol. 56, 69–88.

France-Lanord, C., Derry, L.A., 1994. d13C of organic carbon in the Bengal Fan: source evolution and transport of $C_3$ and $C_4$ plant carbon to marine sediments. Geochim. Cosmochim. Acta 58, 4809–4814.
Freeman, K.H., Colarusso, L.A., 2001. Molecular and isotopic records of $C_4$ grassland expansion in the Late Miocene. Geochim. Cosmochim. Acta 65, 1439–1454.
Galy, V., Francois, L., France-Lanord, C., Faure, P., Kudrass, H., Palhol, F., Singh, S.K., 2008. $C_4$ plants decline in the Himalyan Basin since the Last Glacial Maximum. Quat. Sci. Rev. 27, 1396–1409.
Gardner, J.V., Malik, M.A., Walker, S., 2009. Plume 1400 meters high discovered at the seafloor off the Northern California Margin. EOS Trans. Am. Geophys. Union 90 (32), 275.
Ginsburg, G.D., Soloviev, V.A., 1998. Submarine Gas Hydrates. VNII Okeangeologia, St. Petersburg.
Heeschen, K.U., Trehu, A.M., Collier, R.W., Suess, E., Rehder, G., 2003. Distribution and height of methane bubble plumes on the Cascadia margin characterized by acoustic imaging. Geophys. Res. Lett. 30, 1643–1646.
Hong, W.-L., Torres, M.E., Kim, J.-H., Choi, J., Bahk, J.-J., 2013. Carbon cycling within the sulfate-methane transition-zone in marine sediments from the Ulleung Basin. Biogeochemistry 1–20.
Hong, W.-L., Torres, Marta E., Kim, Ji-Hoon, Choi, Jiyoung, Bahk, Jang-Jun, 2014a. Towards quantifying the reaction network around the sulfate–methane-transition-zone in the Ulleung Basin, East Sea, with a kinetic modeling approach. Geochim. Comochim. Acta 140, 127–141. http://dx.doi.org/10.1016/j.gca.2014.05.032.
Hong, W.-L., Solomon, E.A., Torres, M.E., 2014b. A kinetic-model approach to quantify the effect of mass transport deposits on pore water profiles in the Krishna–Godavari Basin, Bay of Bengal. Mar. Pet. Geol. 58, 223–232.
Jablonski, S.A., Mecray, E.L., Munson, J.M., Blackwood, D.S., 2002. CHN preparation and analysis. In: Geochemical Analysis Procedures: U.S. Geological Survey Open-file Report 02–371. http://pubs.usgs.gov/of/2002/of02-371/chnmeth.htm.
Jaiswal, P., Dewangan, P., Ramprasad, T., Zelt, C.A., 2012. Seismic characterization of hydrates in faulted, fine-grained sediments of Krishna–Godavari Basin: full waveform inversion. J. Geophys. Res. 117, B10305. http://dx.doi.org/10.1029/2012JB009201.
Kalaswad, S., Roden, M.K., Miller, D.S., Morisawa, M., 1993. Evolution of the continental margin of Western India: new evidence from apatite-fission-track dating. J. Geol. 101, 667–673.
Karig, D.E., Lawrence, M.B., Moore, G.F., Curray, J.R., 1980. Structural framework of the fore-arc basin, NW Sumatra. J. Geol. Soc. Lond. 137, 77–91.
Kastner, M., 2001. Gas hydrates in convergent margins: formation, occurrence, geochemistry and global significance. AGU Geophys. Monogr. 124, 67–86.
Kessarkar, P.M., Rao, V.P., Ahmad, S.M., Babu, G.A., 2003. Clay minerals and Sr-Nd isotopes of the sediments along the western margin of India and their implication for sediment provenance. Mar. Geol. 202, 55–69.
Khan, P.K., Chakraborty, P., 2005. Two-phase opening of Andaman Sea: a new seismotectonic insight. Earth Planet. Sci. Lett. 229, 259–271.
Klauda, J.B., Sandler, S.I., 2005. Global distribution of methane hydrate in ocean sediment. Energ. Fuel 19, 459–470. http://dx.doi.org/10.1021/ef049798o.
Kolla, V., Biscaye, P., 1973. Clay mineralogy and sedimentation in the eastern Indian Ocean. Deep Sea Res. 20, 727–738.
Kvenvolden, K.A., 1993. Gas hydrates-geological perspective and global change. Rev. Geophys. 31 (2), 173–187.
Kvenvolden, 1995. A review of the geochemistry of methane in natural gas hydrate. Org. Geochem. 23 (11112), 997–1008.
Lee, M.W., Collett, T.S., 2009. Gas hydrate saturations estimated from fractured reservoir at Site NGHP-01-10, Krishna–Godavari Basin, India. J. Geophys. Res. 114, B07102. http://dx.doi.org/10.1029/2008JB006237.
Liu, X., Flemings, P.B., 2006. Passing gas through the hydrate stability zone at southern Hydrate Ridge, offshore Oregon. Earth Planet. Sci. Lett. 241, 211–226.
Liu, X., Flemings, P.B., 2007. Dynamic multiphase flow model of hydrate formation in marine sediments. J. Geophys. Res. 112, B03101. http://dx.doi.org/10.1029/2005JB004227.
Lorenson, T.D., 2000. Microscopic character of marine sediment containing disseminated gas hydrate: examples from the Blake Ridge and Middle America Trench. Ann. N. Y. Acad. Sci. 912, 189–194.
Martin, K.M., Gulick, S.P.S., Austin Jr., J.A., Berglar, K., Franke, D., Udrekh, 2014. The West Andaman Fault: a complex strain-partitioning boundary at the seaward edge of the Aceh Basin, offshore Sumatra. Tectonics 33, 786–806. http://dx.doi.org/10.1002/2013TC003475.
Mazumdar, A., Dewangan, P., Joäo, H.M., Peketi, A., Khosla, V.R., Kocherla, M., Badesab, F.K., Joshi, R.K., Roxanne, P., Ramamurty, P.B., Karisiddaiah, S.M., Patil, D.J., Dayal, A.M., Ramprasad, T., Hawkesworth, C.J., Avanzinelli, R., 2009. Evidence of paleo-cold seep activity from the Bay of Bengal, offshore India. Geochem. Geophys. Geosyst. 10, Q06005. http://dx.doi.org/10.1029/2008GC002337.
Mazumdar, A., Peketi, A., Joao, H.M., Dewangan, P., Ramprasad, T., 2014. Pore-water chemistry of sediment cores off Mahanadi Basin, Bay of Bengal: possible link to deep seated methane hydrate deposit. Mar. Pet. Geol. 49, 162–175.
Meyers, P.A., 1994. Preservation of elemental and isotopic source identification of sedimentary organic matter. Chem. Geol. 114, 289–302.
Moeremans, R., Singh, S.C., Mukti, M., McArdle, J., Johansen, K., 2013. Seismic images of structural variations along the deformation front of the Andaman–Sumatra subduction zone: implications for rupture propagation and tsunamigenesis. Earth Planet. Sci. Lett. 386 (2014), 75–85.
Moore, G.F., Curray, J.R., Moore, D.G., Karig, D.E., 1980. Variations in geologic structure along the Sunda fore arc, Northeastern Indian Ocean. In: The Tectonic and Geologic Evolution of Southeast Asian Seas and Islands. Geophysical Monograph Series 23, pp. 145–160.
Müller, P.J., Suess, E., 1979. Productivity, sedimentation rate, and sedimentary organic matter in the oceans – I. Organic carbon preservation. Deep-Sea Res. 26A, 1347–1362.
Nielsen, C., Chamot-Rookea, N., Rangin, C., the ANDAMAN Cruise Team, 2004. From partial to full strain partitioning along the Indo-Burmese hyper-oblique subduction. Mar. Geol. 209, 303–327.
Nyak, G.K., Rao, Ch. R., 2002. Structural configuration of Mahanadi Offshore Basin, India: an aeromagnetic study. Mar. Geophys. Res. 23, 471–479.
Pal, T., Chakraborty, P., Gupta, T., Singh, C., 2003. Geodynamic evolution of the outer-arc—forearc belt in the Andaman Islands, the central part of the Burma-Java subduction complex. Geol. Mag. 140, 289–307.
Paull, C.K., Ussler III, W., Borowski, W.S., 1994. Sources of biogenic methane to form marine gas hydrates. In: Sloan, E.D., Happel, J., Hnatow, M.A. (Eds.), International Conference on Natural Gas Hydrates, Annals of the New York Academy of Sciences, vol. 715, pp. 392–409.
Pedersen, R.B., Searle, M.P., Carter, A., Bandopadhyay, P.C., 2010. U–Pb zircon age of the Andaman ophiolite: implications for the beginning of subduction beneath the Andaman–Sumatra arc. J. Geol. Soc. Lond. 167, 1105–1112. http://dx.doi.org/10.1144/0016-76492009-151.
Phillips, S.C., Johnson, J.E., Miranda, E., Disenhof, C., 2011. Improving CHN measurements in carbonate-rich marine sediments. Limnol. Oceanogr. Methods 9, 194–203.
Phillips, S.C., Johnson, J.E., Underwood, M.B., Guo, J., Giosan, L., Rose, K., 2014a. Long-timescale variation in bulk and clay mineral composition of Indian continental margin sediments in the Bay of Bengal. Arabian Sea, and Andaman Sea, Mar. Pet. Geol. 58, 117–138. Available online 22 July 2014, ISSN 0264-8172. http://dx.doi.org/10.1016/j.marpetgeo.2014.06.018.
Phillips, S.C., Johnson, J.E., Giosan, L., Rose, K., 2014b. Monsoon-influenced variation in productivity and lithogenic sediment flux since 110 ka in the offshore Mahanadi Basin, northern Bay of Bengal. Mar. Pet. Geol. 58, 502–525. Available online 22 May 2014, ISSN 0264-8172. http://dx.doi.org/10.1016/j.marpetgeo.2014.05.007.
Pohlman, J.W., Canuel, E.A., Chapman, N.R., Spence, G.D., Whiticar, M.J., Coffin, R.B., 2005. The origin of thermogenic gas hydrates on the northern Cascadia Margin as inferred from isotopic ($^{13}C/^{12}C$ and D/H) and molecular composition of hydrate and vent gas. Org. Geochem. 36 (5), 703–716.
Pohlman, J.W., Kaneko, M., Heuer, V.B., Coffin, R.B., Whiticar, M., 15 2009. Methane sources and production in the northern Cascadia margin gas hydrate system. Earth Planet. Sci. Lett. 287 (3–4), 504–512.
Ponton, C., Giosan, L., Eglinton, T.I., Fuller, D.Q., Johnson, J.E., Kumar, P., Collett, T.S., 2012. Holocene aridification of India. Geophys. Res. Lett. 39, L03704. http://dx.doi.org/10.1029/2011GL050722.
Powell, C.M., Roots, S.R., Veevers, J.J., 1988. Pre-breakup continental extension in East Gondwanaland and the early opening of the eastern Indian Ocean. Tectonophysics 155, 261–283.
Prakash, Samanta, Singh, 2010. A seismic study to investigate the prospect of gas hydrate in Mahanadi deep water basin, northeastern continental margin of India Margin. Geophys. Res. 31 (2010), 253–262. http://dx.doi.org/10.1007/s11001-010-9106-9.
Radhakrishna, M., Twinkle, D., Nayak, S., Bastia, R., Rao, G.S., 2012. Crustal structure and rift architecture across the Krishna–Godavari basin in the central Eastern Continental Margin of India based on analysis of gravity and seismic data. Mar. Pet. Geol. 37 (1), 129–146. http://dx.doi.org/10.1016/j.marpetgeo.2012.05.005.
Rajan, A., Mienert, J., Bünz, S., Chand, S., 2012. Potential serpentinization, degassing, and gas hydrate formation at a young (<20 Ma) sedimented ocean crust of the Arctic Ocean ridge system. J. Geophys. Res. 117, B03102. http://dx.doi.org/10.1029/2011JB008537.
Raju, K.A., Ramprasad, T., Rao, P., Rao, B., Varghese, J., 2004. New insights into the tectonic evolution of the Andaman basin, northeast Indian Ocean. Earth Planet. Sci. Lett. 221, 145–162.
Raju, K.A., Murty, G., Amarnath, D., Kumar, M., 2007. The west Andaman fault and its influence on the aftershock pattern of the recent megathrust earthquakes in the Andaman-Sumatra region. Geophys. Res. Lett. 34, 1–5.
Raju, S.V., Sharma, D., June 2006. Origin and nature of natural gases with special reference to the hydrocarbon gases from offshore east coast basins of India. J. Petrotech Soc. 14–25.
Ramana, M.V., Ramprasad, T., Maria, Desa, 2001. Seafloor spreading magnetic anomalies in the Enderby basin, East Antarctica. Earth Planet. Sci. Lett. 191, 241–255.
Ramana, M.V., Ramprasad, T., Paropkari, A.L., Borole, D.V., Rao, B.R., Karisiddaiah, S.M., Desa, M., Kocherla, M., Joao, H.M., Lokabharati, P., Gonsalves, M.-J., Pattan, J.N., Khadge, N.H., Babu, C.P., Sathe, A.V., Kumar, Sethi, A.K., 2009. Multidisciplinary investigations exploring indicators of gas hydrate occurrence in the Krishna–Godavari Basin offshore, east coast of India. Geo-Mar. Lett. 29, 25–38.
Ramaswamy, V., et al., 1991. Lithogenic fluxes to the deep Arabian Sea measured by sediment traps. Deep-Sea Res. 38, 169–184.
Ramaswamy, V., Gaye, B., Shirodkar, P.V., Rao, P.S., Chivas, A.R., Wheeler, D., Thwin, S., 2008. Distribution and sources of organic carbon, nitrogen and their isotopic signatures in sediments from the Ayeyarwady (Irrawaddy) continental shelf, northern Andaman Sea. Mar. Chem. 111, 137–150.
Ramprasad, T., Dewangan, P., Ramana, M.V., Mazumdar, A., Karisiddaiah, S.M., Ramya, E.R., Sriram, G., 2011. Evidence of slumpin/sliding in Krishna–Godavari offshore basin due to gas/fluid movements. Mar. Pet. Geol. 28, 1806–1816.

Rao, V.P., Rao, B.R., 1995. Provenance and distribution of clay minerals in the sediments of the western continental shelf and slope of India. Cont. Shelf Res. 14, 1757–1771.

Rees, E.V.L., Priest, J.A., Clayton, C.R.I., 2011. The structure of methane gas hydrate bearing sediments from the Krishna–Godavari Basin as seen from Micro-CT scanning. Mar. Pet. Geol. 28, 1283–1293.

Rickers, K., Mezger, K., Raith, M.M., 2001. Evolution of the continental crust in the Proterozoic Eastern Ghats Belt, India and new constraints for Rodinia reconstruction: implications from Sm-Nd, Rb-Sr and Pb-Pb isotopes. Precambrian Res. 112, 183–210.

Riedel, M., Collett, T.S., Kumar, P., Sathe, A.V., Cook, A., 2010. Seismic imaging of a fractured gas hydrate system in the Krishna–Godavari Basin offshore India. Mar. Pet. Geol. ISSN: 0264-8172 27 (7), 1476–1493. http://dx.doi.org/10.1016/j.marpetgeo.2010.06.002.

Riedel, M., Collett, T.S., Shankar, U., 2011. Documenting channel features associated with gas hydrates in the Krishna–Godavari Basin, offshore India. Mar. Geol. 279, 1–11.

Rodolfo, K., 1969. Bathymetry and marine geology of the Andaman Basin, and tectonic implications for Southeast Asia. Geol. Soc. Am. Bull. 80, 1203–1230.

Rodolfo, K., 1975. The Irrawady Delta: tertiary setting and modern offshore sedimentation. Deltas Models Explor. 339–356.

Rose, K.K., Johnson, J.E., Torres, M.E., Hong, W.-L., Giosan, L., Solomon, E.S., Kastner, M., Cawthern, T., Long, P.E., Schaef, H.T., 2014. Anomalous porosity preservation and preferential accumulation of gas hydrate in the Andaman Accretionary Wedge, NGHP-01 Site 17A. Mar. Pet. Geol. 58, 99–116. Available online 6 June 2014, ISSN 0264-8172. http://dx.doi.org/10.1016/j.marpetgeo.2014.04.009.

Royer, J.Y., et al., 2002. Paleogene plate tectonic evolution of the Arabian and Eastern Somali basins. In: Clift, P., et al. (Eds.), The Tectonic and Climatic Evolution of the Arabian Sea Region. Geological Society, London, pp. 7–23.

Schlich, R., 1981. Aseismic ridges, spreading centers, and ocean basins. In: Nairn, A.E.M., Stehli, F.G. (Eds.), The Indian Ocean. Plenum Press, New York, pp. 51–148.

Shankar, U., Riedel, M., 2011. Gas hydrate saturation in the Krishna–Godavari basin from P-wave velocity and electrical resistivity logs. Mar. Pet. Geol. 28, 1768–1778.

Shankar, U., Riedel, M., 2014. Assessment of gas hydrate saturation in marine sediments from resistivity and compressional-wave velocity log measurements in the Mahanadi Basin, India. Mar. Pet. Geol. 58, 265–277. Available online 31 October 2013, ISSN 0264-8172. http://dx.doi.org/10.1016/j.marpetgeo.2013.10.007.

Shanmugam, G., Shrivastava, S.K., Das, B., 2009. Sandy debrites and tidalites of Pliocene reservoir sands in upper-slope canyon environments, offshore Krishna–Godavari Basin (India): implications. J. Sediment. Res. 79, 736–756.

Sloan, E.D., Koh, C.A., 2008. Clathrate Hydrates of Natural Gases, third ed. CRC Press. 721 pp.

Smith, A.J., Mienert, J., Bünz, S., Greinert, J., 2014. Thermogenic methane injection via bubble transport into the upper Arctic Ocean from the hydrate-charged Vestnesa Ridge, Svalbard. Geochem. Geophys. Geosyst. 15, 1945–1959. http://dx.doi.org/10.1002/2013GC005179.

Solomon, E., Spivack, A.J., Kastner, M., Torres, M.E., Robertson, G., 2014. Gas hydrate distribution and carbon sequestration through coupled microbial methanogenesis and silicate weathering in the Krishna–Godavari basin, offshore India. J. Marine Pet. Geol. 58, 233–253. SI India Gas Hydrates Available online 6 September 2014, ISSN 0264-8172. http://dx.doi.org/10.1016/j.marpetgeo.2014.08.020.

Stein, R., 1990. Organic carbon content/sedimentation rate relationship and its paleoenvironmental significance for marine sediments. Geo Mar. Lett. 10, 37–44.

Subrahmanyam, C., Chand, S., 2006. Evolution of the passive continental margins of India—a geophysical appraisal. Gondwana Res. 10 (2006), 167–178.

Subramanian, V., 1980. Mineralogical input of suspended matter by Indian rivers into the adjacent areas of the Indian Ocean. Mar. Geol. 36, 29–34.

Teichert, B.M.A., Johnson, J.E., Solomon, E.A., Giosan, L., Rose, K., Kocherla, M., Connolly, E.C., Torres, M.E., 2014. Composition and origin of authigenic carbonates in the Krishna-Godavari and Mahanadi Basins, eastern continental margin of India. Mar. Pet. Geol. 58, 438–460. Available online 19 September 2014, ISSN 0264-8172. http://dx.doi.org/10.1016/j.marpetgeo.2014.08.023.

Torres, M.E., Wallmann, K., Trehu, A.M., Bohrmann, G., Borowski, W.S., Tomaru, H., 2004. Reply to comment: gas hydrate growth, methane transport, and chloride enrichment at the southern summit of Hydrate Ridge, Cascadia margin off Oregon. Earth Planet. Sci. Lett. 239, 168–175.

Torres, M.E., Tréhu, A.M., Cespedes, N., Kastner, M., Wortmann, U.G., Kim, J.-H., Long, P., Malinverno, A., Pohlman, J.W., Riedel, M., Collett, T., 2008. Methane hydrate formation in turbidite sediments of northern Cascadia, IODP Expedition 311. Earth Planet. Sci. Lett. 271 (1–4), 170–180.

Torres, M.E., Kim, J.-H., Choi, J., Ryu, J.-B., Bahk, J.-J., Riedel, M., Collett, T., Hong, W.-L., Kastner, M., 2011. Occurrence of high salinity fluids associated with massive near-seafloor gas hydrate deposits. In: Proceedings of the 7th International Conference on Gas Hydrates (ICGH 2011), Edinburgh, Scotland, United Kingdom, July 17–21, 2011.

Tréhu, A.M., Flemings, P.B., Bangs, N.L., Chevallier, J., Gracia, E., Johnson, J.E., Liu, C.-S., Liu, X., Riedel, M., Torres, M.E., 2004. Feeding methane vents and gas hydrate deposits at south Hydrate Ridge. Geophys. Res. Lett. 31, L23310. http://dx.doi.org/10.1029/2004GL021286.

Verardo, D.J., Froelich, P.N., McIntyre, A., 1990. Determination of organic carbon and nitrogen in marine sediments using the Carlo Erba NA-1500 Analyzer. Deep-Sea Res. 37, 157–165.

Wallmann, K., Pinero, E., Burwicz, E., Haeckel, M., Hensen, C., Dale, A.W., Ruepke, L., 2012. The global inventory of methane hydrate in marine sediments: a theoretical approach. Energies 5 (7), 2449–2498. http://dx.doi.org/10.3390/en5072449.

Waseda, A., 1998. Organic carbon content, bacterial methanogenesis, and accumulation process of gas hydrates in marine sediments. Geochem. J. 32, 143–157.

Waseda, A., Uchida, T., 2004. The geochemical context of gas hydrate in the Eastern Nankai Trough. Resour. Geol. 54, 69–78. http://dx.doi.org/10.1111/j.1751-3928.2004.tb00188.x.

Weber, T.C., Mayer, L., Jerram, K., Beaudoin, J., Rzhanov, Y., Lovalvo, D., 2014. Acoustic estimates of methane gas flux from the seabed in a 6000 $km^2$ region in the Northern Gulf of Mexico. Geochem. Geophys. Geosyst. 15, 1911–1925. http://dx.doi.org/10.1002/2014GC005271.

Whiticar, M.J., 1999. Carbon and hydrogen isotope systematics of bacterial formation and oxidation of methane. Chem. Geol. 161, 291–314.

Xie, S.-P., et al., 2006. Role of narrow mountains in large-scale organization of Asian monsoon convection. J. Clim. 19 (14), 3420–3429. http://dx.doi.org/10.1175/jcli3777.1.

Xu, W., Ruppel, C., 1999. Predicting the occurrence, distribution, and evolution of methane gas hydrate in porous marine sediments. J. Geophys. Res. 104, 5081–5095.